Emittance Dilutions in Linac-Based Free-Electron Lasers

LCLS-II-TN-22-04

11/17/22

Paul Emma (SLAC) and Marco Venturini (LBNL)

December 6, 2017

Emittance Dilutions in Linac-Based Free-Electron Lasers*

P. Emma
SLAC National Accelerator Laboratory
M. Venturini
Lawrence Berkeley National Laboratory

Abstract

A formalism for the evaluation of transverse emittance dilution due to single component errors in a single-pass electron linac or transport line is presented, and with the introduction of the 'equivalent' emittance, which takes into account not only the increase of the phase space area, but also the associated phase space distortion or matching error. Many specific dilution mechanisms are identified here, such as dispersion errors, misaligned magnets, magnet field quality errors, synchrotron radiation, and wakefields, with simple analytical formulas developed for each case. In many cases actual emittance measurements at the LCLS [1] or tracking simulations are compared.

*Work supported by the U.S. Department of Energy under contract DE-AC02-76SF005.

1 Introduction

A revolution in light source technology has recently emerged with the success of the X-ray Free-Electron Laser (FEL) [1], [2], [3]. The X-ray FEL provides nearly ten orders of magnitude increase in photon brightness with respect to third-generation light sources based on storage ring technology. With this exceptionally bright and penetrating radiation, and with femtosecond pulse lengths and Angstrom-scale wavelengths available, many fields of scientific study are making spectacular new advances [**?**]; in molecular imaging, dynamics in biological macromolecules, materials science, atomic physics, ultrafast electron dynamics, and many more disciplines which benefit from high-brightness, ultrashort hard and soft coherent x-ray pulses.

The FEL output power is highly sensitive to the electron beam quality and final energy, with much effort taken to generate and preserve these high brightness electron beams as they are accelerated and transported to the FEL undulator, which produces this coherent radiation. Electron beam emittance preservation in the linear accelerator (linac), as a driver for an FEL [4], is critical to the machine's performance. Various forms of emittance growth occur in the linac, the bunch compressors, and the electron transport lines. These mechanisms define many of the system and component tolerances and need to be fully examined prior to machine construction and operation.

We quantify many common emittance growth mechanisms and in some cases suggest possible corrections. To allow simple analytical expressions for emittance growth due to various errors in a single-pass machine, we concentrate here on the immediate, single component emittance effects and leave the task of evaluating many simultaneous component errors to detailed computer simulations. Central to our discussion is the concept of the 'equivalent emittance' [6], introduced to us by Bill Spence at SLAC in 1991, which quantifies not only the phase space area increase (emittance growth) generated by the error, but also the phase space ellipse distortion (matching error). We quantify these effects by examining the second moments of the phase space distributions immediately following a single component error, such as a misalignment. Note that the results of this analysis are most suitable to evaluating single component tolerances where emittance growth levels need to be held to less than a few percent. For convenience, a table of mathematical symbols is provided in Table 1, and many single component tolerances, based on our formulations here, are plotted for the LCLS machine design as an examaple. Finally, a summary of the emittance growth formulas derived here is listed in Table 2 for convenient reference.

2 Emittance Growth Formalism

2.1 The Sigma Matrix

We describe the transverse phase space of an electron beam in terms of its 2nd moments using the covariance (sigma) matrix [5], starting with the unperturbed ('design') phase space with the standard beam Twiss parameters α_0, β_0, γ_0, where the subscript zero indicates the 'design' values at the location of interest (see Fig. 1). The 2×2 sigma matrix for the design

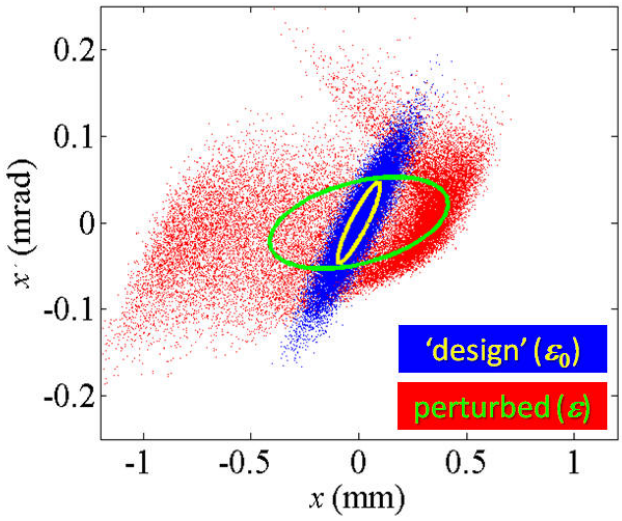

Figure 1: Simulated transverse phase space with the 'design' distribution (blue) and its representative rms ellipse (yellow), and the 'perturbed' distribution (red) and its representative ellipse (green). The ellipses represent the 2nd moments of the distributions (the covariance matrix), even for highly distorted phase space distributions as shown in red.

beam is shown in Eq. (1).

$$\boldsymbol{\sigma}_0 \equiv \begin{pmatrix} \langle x_0^2 \rangle & \langle x_0 x_0' \rangle \\ \langle x_0 x_0' \rangle & \langle x_0'^2 \rangle \end{pmatrix} \equiv \varepsilon_0 \begin{pmatrix} \beta_0 & -\alpha_0 \\ -\alpha_0 & \gamma_0 \end{pmatrix}. \tag{1}$$

Here $\gamma_0 \equiv (1+\alpha_0^2)/\beta_0$, the electrons are relativistic ($E \gg mc^2$), and the brackets, $\langle\rangle$, represent an ensemble average over the electron coordinates within the bunch at one location, and chosen around their mean value such that $\langle x_0 \rangle = 0$ and $\langle x_0' \rangle = 0$. From these second moments, the rms transverse emittance is

$$\varepsilon_0 = \sqrt{\det(\boldsymbol{\sigma}_0)} = \sqrt{\langle x_0^2 \rangle \langle x_0'^2 \rangle - \langle x_0 x_0' \rangle^2}. \tag{2}$$

The rms transverse emittance, an invariant quantity under linear transport, has geometric interpretation as the area/π of the phase space ellipse.

If a perturbation or error is present in the beamline, the resulting beam covariance matrix

$$\boldsymbol{\sigma} \equiv \begin{pmatrix} \langle x^2 \rangle & \langle x x' \rangle \\ \langle x x' \rangle & \langle x'^2 \rangle \end{pmatrix} \equiv \varepsilon \begin{pmatrix} \beta & -\alpha \\ -\alpha & \gamma \end{pmatrix}, \tag{3}$$

will, in general, be different from $\boldsymbol{\sigma}_0$ in Eq. (1). The perturbation may change the emittance, $\varepsilon_0 \to \varepsilon$, the beam Twiss parameters, $\alpha_0 \to \alpha$, $\beta_0 \to \beta$, $\gamma_0 \to \gamma$, or both.

To describe the emittance growth we will write the particle coordinates at the exit of the beamline of interest as $x = x_0 + \Delta x$ and $x' = x_0' + \Delta x'$, where $(\Delta x, \Delta x')$ represents the coordinate perturbation due *e.g.* to optical aberrations, scattering, radiation emission, etc.

The covariance matrix for the perturbed beam can then be written as

$$\boldsymbol{\sigma} = \begin{pmatrix} \langle (x_0 + \Delta x)^2 \rangle & \langle (x_0 + \Delta x)(x_0' + \Delta x') \rangle \\ \langle (x_0 + \Delta x)(x_0' + \Delta x') \rangle & \langle (x_0' + \Delta x')^2 \rangle \end{pmatrix}. \tag{4}$$

2.2 Emittance Growth and Matching Error

For simplicity, and since they describe many important emittance growth mechanisms, we start by considering perturbations that are uncorrelated with the unperturbed phase-space coordinates:

$$\langle x_0 \Delta x \rangle = \langle x_0 \Delta x' \rangle = \langle x_0' \Delta x \rangle = \langle x_0' \Delta x' \rangle = 0. \tag{5}$$

This case encompasses common mechanisms which couple the orthogonal bunch coordinates (y, y', z, or $\delta \equiv \Delta E/E$) into these transverse coordinates (x and x'), such as x-y coupling, transverse wakefields, momentum dispersion, and synchrotron radiation. With the assumption of uncorrelated perturbations, as defined in Eq. (5), the resulting emittance (squared) becomes

$$\varepsilon^2 = \det(\boldsymbol{\sigma}) = \varepsilon_0^2 + \varepsilon_0 \left(\beta_0 \langle \Delta x'^2 \rangle + 2\alpha_0 \langle \Delta x \Delta x' \rangle + \gamma_0 \langle \Delta x^2 \rangle \right) + \varepsilon_a^2, \tag{6}$$

where the additive emittance component is

$$\varepsilon_a^2 = \langle \Delta x^2 \rangle \langle \Delta x'^2 \rangle - \langle \Delta x \Delta x' \rangle^2. \tag{7}$$

This additive emittance component, ε_a, is best understood from Eq. (6) with the unperturbed emittance, ε_0, set to zero. In this case the perturbed emittance is simply the additive emittance, with $\varepsilon_a \geq 0$. Note that the assumption of no correlations in Eq. (5) is important here, since setting the unperturbed emittance, ε_0, to zero would otherwise affect and possibly eliminate the additive emittance, ε_a. For example, the geometric aberrations of a sextupole magnet may vanish if the initial emittance is zero (*i.e.*, no transverse beam spread). The case of finite correlations will be treated in the next sections.

In analogy with Eq. (3) we write the second moments of the perturbation as $\langle \Delta x^2 \rangle = \varepsilon_a \beta_a$, $\langle \Delta x \Delta x' \rangle = -\varepsilon_a \alpha_a$, and $\langle \Delta x'^2 \rangle = \varepsilon_a \gamma_a$, and cast the expression for the emittance of Eq. (6) in the form

$$\varepsilon^2 = \varepsilon_0^2 + 2\zeta_a \varepsilon_0 \varepsilon_a + \varepsilon_a^2, \tag{8}$$

where ζ_a in the cross-term is the beta-mismatch amplitude of the perturbation with respect to the design Twiss functions, defined as

$$\zeta_a \equiv \frac{1}{2} \left(\beta_0 \gamma_a - 2\alpha_0 \alpha_a + \gamma_0 \beta_a \right) \geq 1. \tag{9}$$

This amplitude mismatch parameter is discussed in the next sections.

Note that the Twiss beam parameters, α_0, β_0, and γ_0, describe the nominal ('design') phase space, whereas the parameters, α_a, β_a, and γ_a, describe the additive phase space, as shown in red in Fig. 2. If the additive phase space ellipse (red) matches (*i.e.*, has the same shape and orientation but not necessarily the same area) the unperturbed ellipse (blue), as

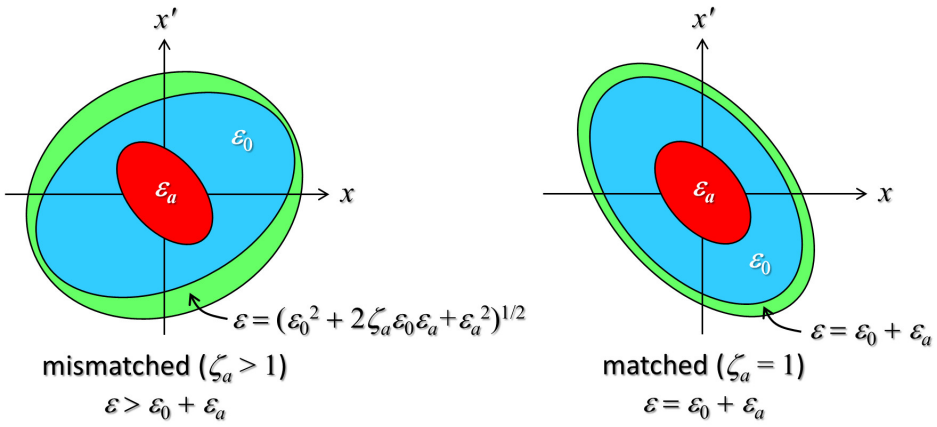

Figure 2: Graphical representation of the phase space showing how an additive emittance (ε_a, red), added to the unperturbed beam ellipse (ε_0, blue), affects the final beam ellipse (ε, green), depending on their relative matching condition, ζ_a. The final emittance at left is larger due to its mismatched condition, $\zeta_a > 1$, whereas the right side shows the minimum perturbed emittance arranged with $\zeta_a = 1$ by choosing the matched initial beam ellipse (blue).

shown in the right plot of Fig. 2, then $\zeta_a = 1$ and the final emittance of Eq. (8) becomes a minimum as a simple sum of the initial and additive emittances:

$$\varepsilon = \varepsilon_0 + \varepsilon_a. \tag{10}$$

However, if the additive phase space ellipse (red) does not match the initial ellipse (blue), as shown in the left plot of Fig. 2, then $\zeta_a > 1$ and Eq. (8) describes the emittance of the perturbed beam, including the cross term, and the perturbed emittance is greater than the sum of the two components: $\varepsilon > \varepsilon_0 + \varepsilon_a$.

So for example, if the synchrotron radiation of a bend magnet generates the red ellipse shown in Fig. 2, one can always readjust the focusing upstream of the bend to transform the blue ellipse to match the red, and the total emittance would then be the minimum (the sum).

Many emittance dilution mechanisms have $\varepsilon_a = 0$. These include (but are not limited to) perturbations that are 'point-like', where the particle kicks may be random in amplitude, but they all occur at the same betatron phase (as shown in the two top plots of Fig. 3), as happens with one thin kick source, such as Coulomb angular scattering in a thin foil.

In this case the position errors, Δx, observed downstream of the kick source are completely correlated with the angle errors, $\Delta x'$, meaning that: $\langle \Delta x \Delta x' \rangle^2 = \langle \Delta x^2 \rangle \langle \Delta x'^2 \rangle$, and the additive emittance, ε_a, in Eq. (7) is then clearly zero (as shown at top-right of Fig. 3), even though we may have non-zero final emittance growth.

For these 'point-like' emittance dilution mechanisms, Eq. (6), with $\varepsilon_a = 0$, becomes

$$\begin{aligned} \varepsilon^2 &= \varepsilon_0^2 + \varepsilon_0 \left(\beta_0 \langle \Delta x'^2 \rangle + 2\alpha_0 \langle \Delta x^2 \rangle^{1/2} \langle \Delta x'^2 \rangle^{1/2} + \gamma_0 \langle \Delta x^2 \rangle \right) \\ &= \varepsilon_0^2 + \frac{\varepsilon_0}{\beta_0} \left(\langle \Delta x^2 \rangle + \left[\alpha_0 \langle \Delta x^2 \rangle^{1/2} + \beta_0 \langle \Delta x'^2 \rangle^{1/2} \right]^2 \right). \end{aligned} \tag{11}$$

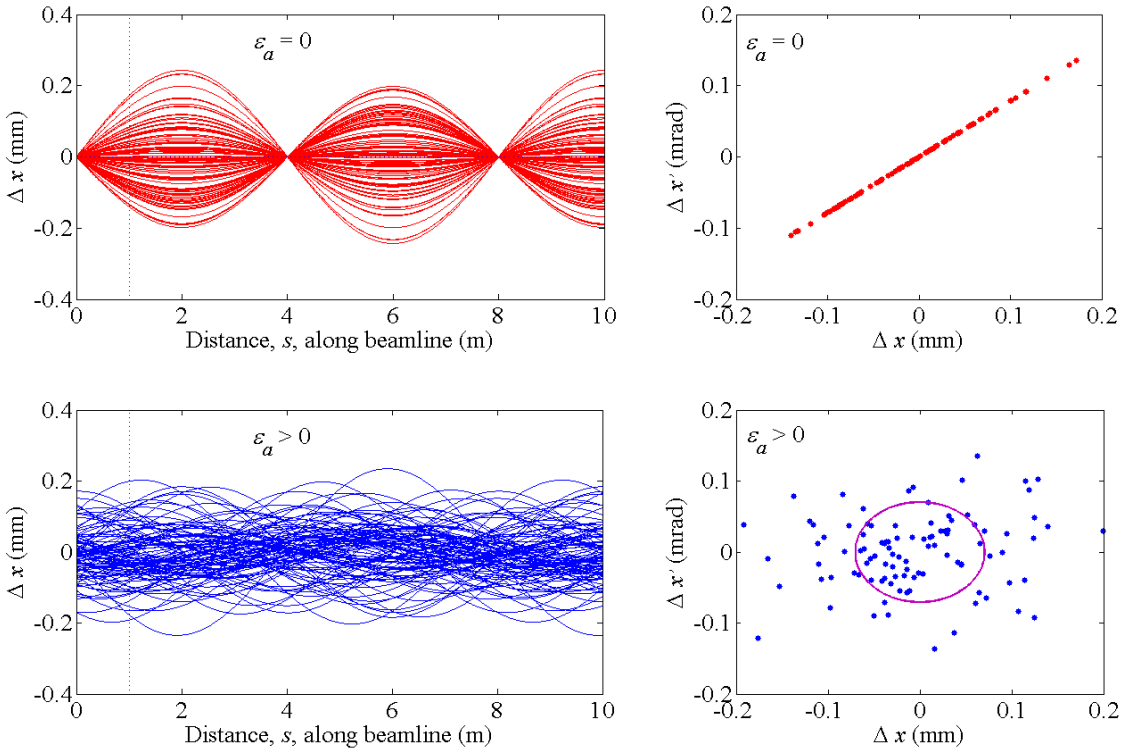

Figure 3: Simplified simulation of 100 electron trajectories, Δx, along the beamline (top-left, red) shown in the case where Δx and $\Delta x'$ are fully correlated (see top-right phase space plot) due to a single upstream thin-kick source, such as a foil. In this 'point-like' case the additive emittance is $\varepsilon_a = 0$ and an ellipse is not defined. The bottom two plots show the case where Δx and $\Delta x'$ are not highly correlated, due to a finite-length perturbation source upstream (*e.g.*, photon emission along a dipole magnet). In this case the additive emittance is $\varepsilon_a > 0$ and the representative rms ellipse is shown (dashed). The two phase space plots at right are sampled at $s = 1$ (the vertical dashed line in the left-side plots) along the beamline in this figure.

In the simplest cases, with only angular kicks ($\Delta x = 0$), Eq. (11) becomes

$$\frac{\varepsilon}{\varepsilon_0} = \sqrt{1 + \frac{\beta_0}{\varepsilon_0}\langle \Delta x'^2 \rangle}, \tag{12}$$

and the effect can be minimized by choosing β_0 as small as possible. We can also examine the case with position scattering, but no angular scattering (although unusual), where $\Delta x' = 0$ (*e.g.*, by evaluating the phase space at $s = 2$ at top-left of Fig. 3, where the kicks have evolved into position-only errors), and then Eq. (11) becomes

$$\frac{\varepsilon}{\varepsilon_0} = \sqrt{1 + \frac{\gamma_0}{\varepsilon_0}\langle \Delta x^2 \rangle}, \tag{13}$$

where again the effect can be minimized by reducing $\gamma_0 = (1 + \alpha_0^2)/\beta_0$ (*e.g.*, setting $\alpha_0 = 0$ and maximizing β_0).

However, if we choose the optimal design Twiss parameters in order to minimize the emittance growth, as suggested above in Eqs. (12) and (13), we will move arbitrarily close to the matched condition ($\zeta_a \to 1$), and in this limit, and with $\varepsilon_a = 0$, the final emittance is not increased at all (see Eq. (10)). However, the chosen design Twiss parameters may have been pushed toward infinite or impractical levels. This condition can be visualized by taking the top-right plot of Fig. 3 (where $\varepsilon_a = 0$) and fitting an ellipse to the highly correlated data points. The ellipse will have arbitrarily small area, with extreme eccentricity and a rotation angle to match the points. Such an ellipse will have an infinite major axis and an arbitrarily small minor axis.

Finally, it is also worth showing the scaling for very large or very small emittance growth. For a large emittance growth, $\varepsilon/\varepsilon_0 \gg 1$, and with only angular kicks, Eq. (12) approximates to

$$1 \ll \frac{\varepsilon}{\varepsilon_0} \approx \sqrt{\frac{\beta_0}{\varepsilon_0}}\langle \Delta x'^2 \rangle^{1/2}, \tag{14}$$

and the relative emittance growth scales linearly with the rms of the angular kicks, $\langle \Delta x'^2 \rangle^{1/2}$. For a small emittance growth, $\varepsilon/\varepsilon_0 - 1 \equiv \Delta\varepsilon/\varepsilon_0 \ll 1$, Eq. (12) becomes

$$1 \gg \frac{\Delta\varepsilon}{\varepsilon_0} \approx \frac{1}{2}\frac{\beta_0}{\varepsilon_0}\langle \Delta x'^2 \rangle, \tag{15}$$

and now the relative emittance growth scales quadratically with the rms of the angular kicks. This form, with $\Delta\varepsilon/\varepsilon_0 \ll 1$, is useful for evaluating tolerances with, *e.g.*, $\Delta\varepsilon/\varepsilon_0 < 1\%$ (see "Examples" section below). This large and small limit scaling can also be done for Eq. (13), position errors only, but it is not shown here.

2.3 Beta Mismatch Parameter

The beta mismatch amplitude parameter [6, 7, 8], defined as

$$\zeta \equiv \frac{1}{2}\left(\beta_0\gamma - 2\alpha_0\alpha + \gamma_0\beta\right) \geq 1, \tag{16}$$

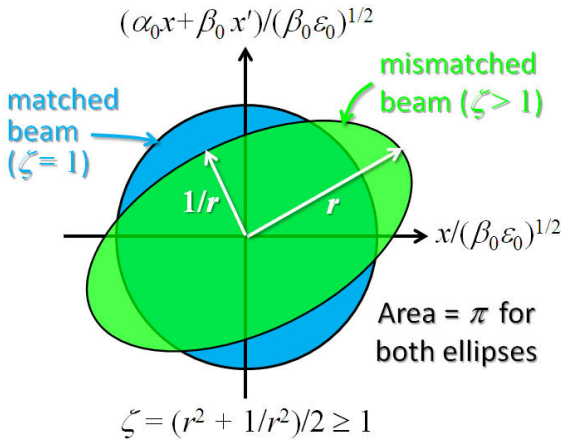

Figure 4: Normalized transverse phase space with two ellipses representing the 2nd moments of two different electron distributions. The mismatch amplitude is $\zeta = 1$ for the matched beam (blue circle), and the mismatched ellipse (green) has $\zeta > 1$, while each ellipse has an area of π. The major and minor axes, r and $1/r$ are also shown for the mismatched ellipse (green) as another way to describe ζ (listed at bottom of figure), and $r = 1$ for the matched ellipse (blue) in these normalized coordinates.

where we drop the a subscript here for more generality, was introduced in Eq. (9) and is a convenient way to measure the amplitude of the beta-mismatch, comparing the perturbed beam (β, α) to the unperturbed (design) lattice functions (β_0, α_0). Substituting $\gamma_0 = (1 + \alpha_0^2)/\beta_0$ and $\gamma = (1 + \alpha^2)/\beta$ into Eq. (16) shows that when $\beta = \beta_0$ and $\alpha = \alpha_0$, then $\zeta = 1$ (the matched condition), and otherwise $\zeta > 1$.

Figure 4 shows the mismatch parameter graphically in normalized phase space for both a matched beam (blue, $\zeta = 1$) and a mismatched beam (green, $\zeta > 1$). Note that a mismatch, $\zeta > 1$, distorts the ellipse but does not change the area if the emittance is preserved. We might also define a mismatch phase [7], based on the ellipse rotation angle, but this is not an important parameter here where we are interested only in evaluation of the emittance growth.

The beta-mismatch amplitude parameter, ζ, is also an invariant under linear transport, as can be easily shown. First notice that the mismatch parameter in Eq. (16) can be written as one half the trace of the product of the perturbed and inverse unperturbed covariance matrices

$$\zeta = \frac{1}{2}\frac{\varepsilon_0}{\varepsilon}\mathrm{Tr}(\boldsymbol{\sigma}\boldsymbol{\sigma}_0^{-1}) = \frac{1}{2}\mathrm{Tr}\left[\begin{pmatrix} \beta & -\alpha \\ -\alpha & \gamma \end{pmatrix}\begin{pmatrix} \gamma_0 & \alpha_0 \\ \alpha_0 & \beta_0 \end{pmatrix}\right]. \tag{17}$$

If now the beam is propagated by a linear transfer matrix $\mathbf{R}$ to some final point downstream of the error source, the covariant matrices evolve as $\boldsymbol{\sigma}_{0f} = \mathbf{R}\boldsymbol{\sigma}_0\mathbf{R}^T$ and $\boldsymbol{\sigma}_f = \mathbf{R}\boldsymbol{\sigma}\mathbf{R}^T$.

The mismatch parameter at the final location is then

$$\begin{aligned} \zeta_f &= \frac{1}{2}\frac{\varepsilon_{0f}}{\varepsilon_f}\mathrm{Tr}(\boldsymbol{\sigma}_f\boldsymbol{\sigma}_{0f}^{-1}) = \frac{1}{2}\frac{\varepsilon_0}{\varepsilon}\mathrm{Tr}(\mathbf{R}\boldsymbol{\sigma}\mathbf{R}^T[\mathbf{R}\boldsymbol{\sigma}_0\mathbf{R}^T]^{-1}) \\ &= \frac{1}{2}\frac{\varepsilon_0}{\varepsilon}\mathrm{Tr}(\mathbf{R}\boldsymbol{\sigma}\boldsymbol{\sigma}_0^{-1}\mathbf{R}^{-1}) = \frac{1}{2}\frac{\varepsilon_0}{\varepsilon}\mathrm{Tr}(\boldsymbol{\sigma}\boldsymbol{\sigma}_0^{-1}) = \zeta, \end{aligned} \tag{18}$$

where in the second equality we have made use of the invariance of the rms emittance under a linear transformation ($\varepsilon_f = \varepsilon$ and $\varepsilon_{0f} = \varepsilon_0$) and later exploited the property of the trace under cyclic permutations of the product of matrices. From Eq. (18) we see that the mismatch amplitude, $\zeta \geq 1$, is invariant over linear beam transport, unless another error arises along the way.

2.4 The Equivalent Emittance

The 'equivalent' rms emittance $\bar{\varepsilon}$ is defined as the product of the rms emittance and the mismatch parameter of the perturbed beam.

$$\bar{\varepsilon} = \zeta\varepsilon \tag{19}$$

In the absence of perturbations, $\varepsilon = \varepsilon_0$, $\zeta = 1$, and the equivalent emittance is the same as the unperturbed emittance $\bar{\varepsilon} = \varepsilon_0$.

The quantity $\bar{\varepsilon} - \varepsilon$ has a compelling physical interpretation as a 'potential' rms emittance growth. Suppose that downstream of the error source, which has changed the unperturbed rms emittance from ε_0 to ε and introduced the mismatch $\zeta > 1$, the beam motion is stable but the transport line has some anharmonicities. Over a long enough beam transport, these will cause the beam to filament and the beam emittance to grow further, toward $\bar{\varepsilon}$. It can be shown [11] that the equivalent emittance is the upper limit to the filamented beam emittance, eventually reached when the beam settles on an equilibrium matched to the lattice. Incidentally, notice that as the product of linearly invariant quantities, the equivalent rms emittance is itself an invariant under linear transport.

From the definition (19) and (16) we have

$$\frac{\bar{\varepsilon}}{\varepsilon_0} = \frac{\varepsilon}{2\varepsilon_0}(\beta_0\gamma - 2\alpha_0\alpha + \gamma_0\beta). \tag{20}$$

Making use of the definitions of the Twiss beam parameters, $\beta = \langle(x_0 + \Delta x)^2\rangle/\varepsilon$, $\alpha = -\langle(x_0 + \Delta x)(x_0' + \Delta x')\rangle/\varepsilon$, and $\gamma = \langle(x_0' + \Delta x')^2\rangle/\varepsilon$, we can rewrite Eq. (20) as

$$\frac{\bar{\varepsilon}}{\varepsilon_0} = \frac{1}{2\varepsilon_0}\left[\beta_0\langle(x_0' + \Delta x')^2\rangle + 2\alpha_0\langle(x_0 + \Delta x)(x_0' + \Delta x')\rangle + \gamma_0\langle(x_0 + \Delta x)^2\rangle\right]. \tag{21}$$

If the correlations of Eq. (5) are all zero, such as produced by an error which generates coupling from an orthogonal bunch coordinate, this reduces to the following expression for the relative equivalent emittance change:

$$\frac{\bar{\varepsilon}}{\varepsilon_0} - 1 \equiv \frac{\Delta\bar{\varepsilon}}{\varepsilon_0} = \frac{1}{2\varepsilon_0}\left(\beta_0\langle\Delta x'^2\rangle + 2\alpha_0\langle\Delta x\Delta x'\rangle + \gamma_0\langle\Delta x^2\rangle\right). \tag{22}$$

We can also recognize the case of the 'point-like' kick, where $\langle\Delta x\Delta x'\rangle^2 = \langle\Delta x^2\rangle\langle\Delta x'^2\rangle$, as shown in Eq. (11), and rewrite this as

$$\frac{\Delta\bar{\varepsilon}}{\varepsilon_0} = \frac{1}{2\varepsilon_0\beta_0}\left[\langle\Delta x^2\rangle + \left(\alpha_0\langle\Delta x^2\rangle^{1/2} + \beta_0\langle\Delta x'^2\rangle^{1/2}\right)^2\right]. \tag{23}$$

For a more general result we will no longer assume uncorrelated initial coordinates, but for simplicity allow for only angular errors, $\Delta x = 0$. Setting $\Delta x = 0$ in (21) we have

$$\frac{\bar{\varepsilon}}{\varepsilon_0} = \frac{1}{2}\frac{\varepsilon}{\varepsilon_0}\left(\beta_0\frac{\langle(x_0' + \Delta x')^2\rangle}{\varepsilon} + 2\alpha_0\frac{\langle x_0(x_0' + \Delta x')\rangle}{\varepsilon} + \gamma_0\frac{\langle x_0^2\rangle}{\varepsilon}\right), \tag{24}$$

which can be reduced to

$$\frac{\Delta\bar{\varepsilon}}{\varepsilon_0} = \frac{1}{2}\frac{\beta_0}{\varepsilon_0}\langle\Delta x'^2\rangle + \frac{\beta_0}{\varepsilon_0}\langle x_0'\Delta x'\rangle + \frac{\alpha_0}{\varepsilon_0}\langle x_0\Delta x'\rangle. \tag{25}$$

We now see the presence of the correlation terms, $\langle x_0'\Delta x'\rangle$ and $\langle x_0\Delta x'\rangle$, which were assumed to be zero in the previous section (see Eq. (5)). If the angular kicks, $\Delta x'$, are due to cross-plane coupling, dispersion, or wakefields, etc., where the kicks are completely uncorrelated with the phase space coordinates, x_0 or x_0', then the two correlation terms in Eq. (25) are each zero and Eq. (25) reduces to Eq. (15), but now exact as the equivalent emittance.

Taking the more general case where $\Delta x'$ is correlated with x_0 (and therefore also correlated with x_0' through a non-zero value of α_0) in the form $\Delta x' = ax_0^n$, such as produced by a quadrupole ($n = 1$), sextupole ($n = 2$), or octupole magnet ($n = 3$), etc., with n as an integer and a an arbitrary constant, and substituting into Eq. (25) we have

$$\frac{\Delta\bar{\varepsilon}}{\varepsilon_0} = \frac{1}{2}\frac{\beta_0}{\varepsilon_0}\langle\Delta x'^2\rangle + a\frac{\beta_0}{\varepsilon_0}\langle x_0'x_0^n\rangle + a\frac{\alpha_0}{\varepsilon_0}\langle x_0^{n+1}\rangle. \tag{26}$$

To show that the two correlation terms on the RHS cancel, we now express x_0' as a sum of x-correlated and x-uncorrelated terms:

$$x_0' = x_u' - \frac{\alpha_0}{\beta_0}x_0, \tag{27}$$

where x_u' is a random coordinate (the intrinsic angular spread), which is by definition uncorrelated with x_0 to all orders ($\langle x_u'x_0^n\rangle = 0$), and the coefficient, $-\alpha_0/\beta_0$, is the standard phase space slope of a tilted ellipse. Substituting Eq. (27) into Eq. (26) gives

$$\frac{\Delta\bar{\varepsilon}}{\varepsilon_0} = \frac{1}{2}\frac{\beta_0}{\varepsilon_0}\langle\Delta x'^2\rangle. \tag{28}$$

This shows that the initial correlations have no effect on the equivalent emittance if we examine the beam at a location where we have angular kicks only ($\Delta x = 0$), such as immediately after a thin-lens error, or the case with both angular and position errors, but these originate from some orthogonal coordinate, such as y, y', z, or δ (*i.e.*, when Eq. (5) holds). These are the conditions we will assume in the sections to follow, where we estimate various emittance growth mechanisms. Note that with this definition, a quadrupole gradient error will increase the equivalent emittance through the matching error, although not an actual rms emittance increase, as we will discuss in the next section.

As mentioned, Eq. (28) is the same as Eq. (15), but now includes the mismatch and is accurate even for large emittance growth. We will use these forms, Eqs. (22), (23), and (28), to evaluate the equivalent emittance increase for various beamline errors, including quadrupole

gradient errors, magnet misalignments, anomalous dispersion, field harmonics, sextupole aberrations, Coulomb scattering, synchrotron radiation, wakefields, etc. The reader should be aware that these formulas may not agree with particle tracking results, especially if the effect is large, unless the equivalent emittance (*e.g.*, Eq. (22)) is calculated, and not the standard emittance of Eq. (6).

For tolerance calculations, where the relative emittance growth for each beamline component must be held to very small levels, the equivalent and standard emittance values are nearly identical, as shown by comparing Eqs. (15) and (28), so there would seem to be little advantage in the use of the equivalent emittance. However, the equivalent emittance is a more general quantity and can easily be calculated without need to work out the various coordinate correlations, such as $\langle x_0 \Delta x' \rangle$, as discussed above. In addition it includes the matching error, which may chromatically filament over a long transport line and become an actual emittance increase. Finally, it allows tolerance estimates on parameters, such as quadrupole magnet gradient errors, which do not impact the emittance directly, but introduce a matching error and a potential to evolve into an increased emittance. These features motivate us to use the equivalent emittance for evaluation of the various dilution mechanisms described in the next sections.

3 Emittance Growth Mechanisms

We now present many examples of emittance dilution mechanisms and calculate the equivalent relative emittance growth for each case. Each of these emittance growth formulas were checked using the particle tracking code *Elegant* [19], or against actual measurements, although not exhaustively, so the expressions should be accurate and hopefully useful to the reader interested in single component emittance growth or tolerance estimates. Note that the expressions are meant to provide a guideline for emittance growth estimates for well-behaved initial beam distributions, and are not meant to cover multiple component errors, or arbitrarily distorted and coupled input beams. In addition, many thin-lens approximations are applied, so some extreme cases, such as the final focusing element of a linear collider, may not be so well suited for this analysis.

3.1 Transverse Momentum Dispersion Errors

3.1.1 First-Order Angular Dispersion

We start with a simple case, such as a strong steering coil with bend angle θ_0, which generates an angular dispersion. Using Eq. (28) with $\Delta x' = -\theta_0 \delta$, where δ is the small ($|\delta| \ll 1$), random, relative energy deviation ($\delta \equiv \Delta E/E$) of each electron with respect to the mean energy. This forms the energy spread in the beam. The equivalent emittance for angular dispersion (*e.g.*, a steering coil of angle θ_0) is

$$\frac{\Delta\bar{\varepsilon}}{\varepsilon_0} = \frac{1}{2}\frac{\beta_0}{\varepsilon_0}\theta_0^2\sigma_\delta^2, \tag{29}$$

where the rms relative energy spread is $\langle\delta^2\rangle^{1/2} \equiv \sigma_\delta$, with $\langle\delta\rangle = 0$. We can also cancel ε_0 on each side, finding $\Delta\bar{\varepsilon} = \frac{1}{2}\beta_0\theta_0^2\sigma_\delta^2$, and showing that this dispersion error generates an additive emittance (not multiplicative), since $\Delta\bar{\varepsilon}$ is independent of ε_0. Such an error might also be attributed to a dipole magnet roll angle error which kicks the beam out of its bend plane. In this case the angle is interpreted as a nominal bend, θ_0, and the out-of-plane kick error in Eq. (29) is replaced as $\theta_0 \to \phi\theta_0$, where ϕ is the (small) roll angle error around the beam direction ($|\phi| \ll 1$). Of course trajectory correction, if applied locally, can remove such a kick.

3.1.2 First-Order Spatial and Angular Dispersion

Moving to a more general case with both spatial, $\Delta\eta$, and angular, $\Delta\eta'$, dispersion errors [6] and using Eq. (22) or (23) with $\Delta x = \Delta\eta\delta$ and $\Delta x' = \Delta\eta'\delta$ we have

$$\frac{\Delta\bar{\varepsilon}}{\varepsilon_0} = \frac{1}{2\varepsilon_0}(\beta_0\Delta\eta'^2 + 2\alpha_0\Delta\eta\Delta\eta' + \gamma_0\Delta\eta^2)\langle\delta^2\rangle. \tag{30}$$

We can also express this using $\gamma_0 = (1+\alpha_0^2)/\beta_0$, and the rms relative energy spread as: $\langle\delta^2\rangle^{1/2} \equiv \sigma_\delta$ and write

$$\frac{\Delta\bar{\varepsilon}}{\varepsilon_0} = \frac{1}{2\beta_0\varepsilon_0}[\Delta\eta^2 + (\alpha_0\Delta\eta + \beta_0\Delta\eta')^2]\sigma_\delta^2. \tag{31}$$

The emittance effect is reversible, as long as no new source of energy spread occurs after the $\Delta\eta$, $\Delta\eta'$ error (*e.g.*, due to an accelerating section which might wash out the energy-x correlations). Dispersion increases the time-projected emittance if the energy spread, σ_δ, is dominantly time-correlated (*e.g.*, a chirped condition). Note that the two quantities $\Delta\eta$ and $(\alpha_0\Delta\eta + \beta_0\Delta\eta')$ have the same units and are in fact the two orthogonal parameters that should be minimized with tuning algorithms, and not the combination $\Delta\eta$ and $\Delta\eta'$, which are independent but not orthogonal (unless $\alpha_0 = 0$).

3.1.3 Second-Order Dispersion

The section above on linear dispersion assumes that the dispersion error introduces a linear correlation within the electron bunch between particle energy and transverse position and/or angle. More complicated optical systems, such as a linear achromat with strong focusing, a sextupole magnet in a bend system, or a quadratic dipole field variation over the transverse dimension in a bend magnet, can generate second-order dispersion [9] with kicks such as $\Delta x' \sim \delta^2$ and/or $\Delta x \sim \delta^2$. To evaluate this effect we again use Eq. (22) with $\Delta x = \Delta\eta_2\delta^2$ and $\Delta x' = \Delta\eta_2'\delta^2$. Here $\Delta\eta_2$ and $\Delta\eta_2'$ are the second-order spatial and angular dispersion errors, respectively (also referred to as the T-matrix elements: T_{166} and T_{266}). Note here that we now have non-zero centroid values, $\langle\Delta x\rangle \sim \langle\delta^2\rangle$, and $\langle\Delta x'\rangle \sim \langle\delta^2\rangle$, so we need to include this mean value in both position and angle by replacing in Eq. (22) the following

$$\begin{aligned}
\langle\Delta x^2\rangle &\to \langle\Delta x^2\rangle - \langle\Delta x\rangle^2 = \Delta\eta_2^2(\langle\delta^4\rangle - \langle\delta^2\rangle^2), \\
\langle\Delta x\Delta x'\rangle &\to \langle\Delta x\Delta x'\rangle - \langle\Delta x\rangle\langle\Delta x'\rangle = \Delta\eta_2\Delta\eta_2'(\langle\delta^4\rangle - \langle\delta^2\rangle^2), \\
\langle\Delta x'^2\rangle &\to \langle\Delta x'^2\rangle - \langle\Delta x'\rangle^2 = \Delta\eta_2'^2(\langle\delta^4\rangle - \langle\delta^2\rangle^2).
\end{aligned} \tag{32}$$

Now we need to know the fourth moment and the square of the second moment of the energy distribution, $\langle\delta^4\rangle$ and $\langle\delta^2\rangle^2 = \sigma_\delta^4$. Evaluating the fourth moment requires knowledge of the energy distribution, so will start by assuming a uniform distribution where $\langle\delta^4\rangle = \frac{9}{5}\sigma_\delta^4$. With this choice, the equivalent emittance for a second-order dispersion error (in position and angle), using Eq. (22), but modified for non-zero mean values as described above, is

$$\frac{\Delta\bar{\varepsilon}}{\varepsilon_0} = \frac{2}{5}\frac{1}{\beta_0\varepsilon_0}[\Delta\eta_2^2 + (\alpha_0\Delta\eta_2 + \beta_0\Delta\eta_2')^2]\sigma_\delta^4, \tag{33}$$

which is additive and reversible, affecting only the time-projected emittance if the beam is chirped and has an insignificant intrinsic energy spread. For comparison, a Gaussian δ-distribution has a fourth moment which is related to the square of its second moment as $\langle\delta^4\rangle = 3\sigma_\delta^4$ and the factor 2/5 in Eq. (33) is replaced by 1 for a Gaussian energy profile. Note that in this treatment the specific distribution functions are only needed when higher than second moments arise, and we will apply symmetric distributions, such as Gaussian and uniform, which have odd moments that are zero (*e.g.*, $\langle\delta^3\rangle = 0$).

3.1.4 Third-Order Dispersion

We can do the same analysis for third-order dispersion (since we have real measurements for this case), again using Eq. (22) and now with $\Delta x = \Delta\eta_3\delta^3$ and $\Delta x' = \Delta\eta_3'\delta^3$, where $\Delta\eta_3$ and $\Delta\eta_3'$ are third-order dispersion errors (also referred to as U-matrix elements: U_{1666} and U_{2666}). Assuming a uniform energy distribution where $\langle\delta^6\rangle = \frac{27}{7}\sigma_\delta^6$ and $\langle\delta^3\rangle = 0$ (which now sets $\langle\Delta x\rangle = \langle\Delta x'\rangle = 0$) we have the equivalent emittance for a third-order dispersion error as

$$\frac{\Delta\bar{\varepsilon}}{\varepsilon_0} = \frac{27}{14}\frac{1}{\beta_0\varepsilon_0}[\Delta\eta_3^2 + (\alpha_0\Delta\eta_3 + \beta_0\Delta\eta_3')^2]\sigma_\delta^6, \tag{34}$$

which is also additive and reversible, typically affecting only the time-projected emittance. For comparison, a Gaussian δ-distribution has third and sixth moments: $\langle\delta^3\rangle = 0$ and $\langle\delta^6\rangle = 15\sigma_\delta^6$, replacing the factor 27/14 in Eq. (34) with 15/2 for a Gaussian energy distribution. Figure 5 [10] shows an example emittance optimization in the SLAC linac using octupole magnets to cancel anomalous third-order dispersion errors coming from the SLC bunch compressor (as described in the caption). Note that Eq. (34) predicts quite well the equivalent emittance increase, $\bar{\varepsilon}$, but Fig. 5 shows the standard emittance, ε. However, it is clear comparing Eqs. (15) and (28) that for a small relative emittance increase the equivalent emittance growth is approximately the same as the standard emittance growth.

3.2 Quadrupole Magnet Gradient Error

Although not a cause of immediate emittance growth, it is useful to examine the effect of a quadrupole magnet field gradient error on the equivalent emittance to get an estimate of its sensitivity, for example, against power supply current regulation errors or field calibration. To be general, we assume the quadrupole magnet is located at a point in the beamline which includes horizontal bend magnets, so the electron's horizontal position in the quadrupole magnet has a contribution, x, from the initial emittance, and a component,

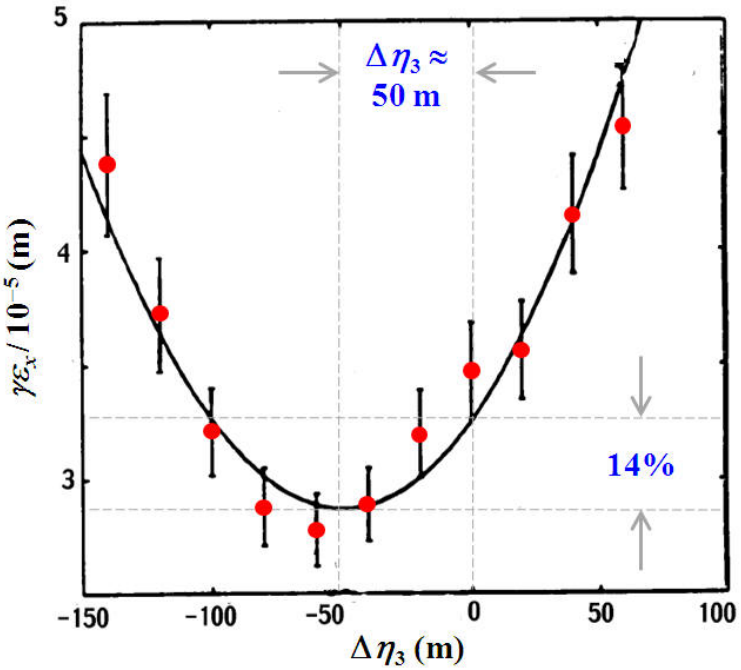

Figure 5: Measured horizontal (normalized) emittance versus third-order spatial dispersion, $\Delta\eta_3$, adjusted using a pair of octupole magnets in the SLC bunch compressor. A linear combination of octupole magnet settings is calibrated in meters of third-order spatial dispersion after the compressor, at the start of the SLAC linac. The observed emittance reduction (from $\Delta\eta_3 = 0$ to $\Delta\eta_3 = -50$ m) is 14%, while Eq. (34) predicts 16%. The beam parameters are: $E \approx 1.2$ GeV, $\gamma\varepsilon_0 \approx 28$ μm, $\beta_0 \approx 3$ m, and the collimated energy profile is approximately uniform here with rms value of $\sigma_\delta \approx 1\%$.

$\eta\delta$, from the dispersion of the electron's small energy deviation, forming random kick errors, $\Delta x' = \frac{\Delta G}{G_0}(x_0 + \eta\delta)/f_0$, where f_0 is the quadrupole magnet's focal length at $\delta = 0$ (ignoring 2nd-order effects for now), and $\Delta G/G_0$ is the small relative gradient error of the magnet with respect to its design setting. We also assume a thin-lens quadrupole (focal length much longer than magnetic length) and write η here as the nominal 'design' dispersion, as opposed to $\Delta\eta$ which indicates a dispersion error. Note that by explicitly separating the initial horizontal position into x_0 and $\eta\delta$ contributions, the correlation term, $\langle x_0\delta\rangle$, is zero by definition, and this definition is used throughout this article. Note also that we have a correlation case here, where $\langle x_0\Delta x'\rangle \neq 0$, breaking Eq. (5), and requiring the use of the equivalent emittance, which is valid even with such correlations.

Since $\Delta x = 0$ here (*i.e.*, only angular kick errors immediately after the thin-lens quadrupole magnet), we use Eq. (28) to calculate the equivalent emittance of a quadrupole gradient error, and to be more clear we also begin labeling parameters as horizontal, x, or vertical, y, at this point, since some errors affect both planes simultaneously.

$$\frac{\Delta\bar{\varepsilon}_x}{\varepsilon_{x0}} = \frac{1}{2}\left(\frac{\Delta G}{G_0}\right)^2 \frac{\beta_{x0}^2}{f_0^2}(1+\xi^2) \tag{35}$$

$$\frac{\Delta\bar{\varepsilon}_y}{\varepsilon_{y0}} = \frac{1}{2}\left(\frac{\Delta G}{G_0}\right)^2 \frac{\beta_{y0}^2}{f_0^2} \tag{36}$$

Here the following definition of ξ^2 is introduced (below) with η always defined as the horizontal (bend-plane) nominal dispersion function at the component of interest (*i.e.*, the nominal vertical dispersion is always assumed to be zero).

$$\xi^2 \equiv \frac{\eta^2\sigma_\delta^2}{\beta_{x0}\varepsilon_{x0}} \tag{37}$$

The quantity, ξ^2, characterizes the beam in the horizontal plane (bend-plane) as either dispersion dominated ($\xi^2 \gg 1$) or emittance dominated ($\xi^2 \ll 1$), and Eq. (35) is valid in either case. Gradient errors are multiplicative ($\Delta\bar{\varepsilon}$ proportional to ε_0), unless $\xi^2 \gg 1$, and reversible if corrected before chromatic filamentation occurs [11] (a washing out of initial correlations due to beam propagation in a long transport line with a finite energy spread). Of course, the gradient error also affects the vertical plane and this is indicated in Eq. (36), scaled with the vertical beta function, β_{y0}. Finally, if the quadrupole magnet has a nominal gradient of zero ($G_0 = 0$), for example a small tuning magnet in a chicane included to allow empirical dispersion correction, then Eq. (35) and (36) can still be used by setting $\Delta G/G_0 = 1$ and using the quadrupole's finite focal length setting, f_0, to estimate the equivalent emittance growth.

3.3 Magnet Alignment Errors

3.3.1 Quadrupole Magnet Transverse Offset

Magnet alignment is critical in linac-based FELs with small errors potentially building up to a large emittance growth and mismatch. It is worth developing a single magnet sensitivity estimate so that the more problematic magnets are identified and possibly mitigated early.

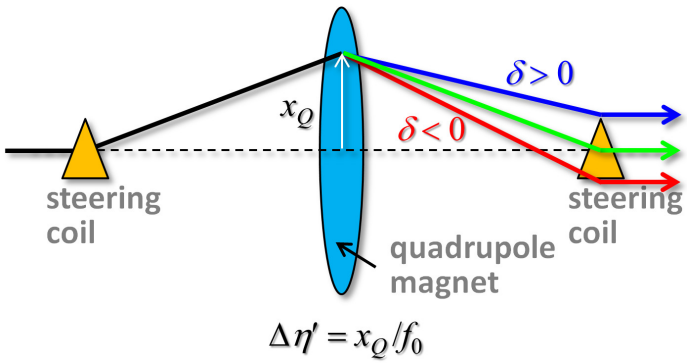

Figure 6: An example quadrupole magnet offset with steering coils use to correct the orbit, leaving only the dispersion generated by the quadrupole. Such a case may arise after trajectory correction if the beam position monitor in the quadrupole were offset by x_Q.

A small transverse offset, x_Q, of a quadrupole magnet introduces a dispersion error, $\Delta x' = -x_Q\delta/f_0$, where f_0 is its nominal focal length, and δ represents the first-order energy dependence of the quadrupole focal length, $f = f_0(1+\delta)$. Of course the magnet misalignment also steers the beam centroid and so we assume, for simplicity, the electron trajectory is corrected in such as way as to leave only the dispersion error from the quadrupole itself, as shown in Fig. 6. More complicated scenarios are possible, with dispersion-free steering or cases where the steering coils add to the dispersion error, but we use this simple, and not unrealistic case to allow quick estimates of quadrupole magnet alignment tolerances. The equivalent emittance for a horizontally offset quadrupole magnet is calculated using Eq. (28), where we assume the following initial correlations are zero: $\langle xy\rangle = 0$ (no initial coupling), $\langle x\delta\rangle = 0$ (by definition of η), and $\langle y\delta\rangle = 0$ (by assuming no vertical bend magnets).

$$\frac{\Delta\bar{\varepsilon}_x}{\varepsilon_{x0}} = \frac{1}{2}\frac{\beta_{x0}}{\varepsilon_{x0}}\left(\frac{x_Q}{f_0}\right)^2\sigma_\delta^2 \tag{38}$$

The equivalent emittance is dependent on the square of the misalignment, the square of the focal length, and the square of the relative energy spread. The effect is additive, reversible, and typically impacts the projected emittance, exactly as in the case of Eq. (29). The vertical emittance growth for a vertical misalignment, y_Q, is identical to Eq. (38) by replacing all x with y.

3.3.2 Quadrupole Magnet Roll Angle

A quadrupole magnet may also have a roll angle error (rotated around the beam direction by ϕ). This generates x-y coupling in the beam and has an impact on the emittance in both planes. Assuming the quadrupole is, again, located in a horizontal bend section ($\eta \neq 0$), the kicks in the vertical plane are $\Delta y' = \sin(2\phi)(x_0 + \eta\delta)/f_0$, and in the horizontal plane $\Delta x' = -\sin(2\phi)y_0/f_0$ (assuming a thin-lens quad and only horizontal dispersion present in the design optics). Note that y_0 is the vertical position coordinate of an electron entering the magnet, and the case with $\phi = \pm\pi/4$ converts this normal quad to a skew quad. The

equivalent emittances in each plane for a rolled quadrupole magnet are calculated using Eq. (28).

$$\frac{\Delta\bar{\varepsilon}_x}{\varepsilon_{x0}} = \frac{1}{2}\sin^2(2\phi)\frac{\beta_{x0}\beta_{y0}}{f_0^2}\left(\frac{\varepsilon_{y0}}{\varepsilon_{x0}}\right) \tag{39}$$

$$\frac{\Delta\bar{\varepsilon}_y}{\varepsilon_{y0}} = \frac{1}{2}\sin^2(2\phi)\frac{\beta_{x0}\beta_{y0}}{f_0^2}\left(\frac{\varepsilon_{x0}}{\varepsilon_{y0}}\right)\left(1+\xi^2\right) \tag{40}$$

Here ε_{x0} and ε_{y0} are the initial horizontal and vertical emittance values before the rolled magnet, respectively, and ξ^2 is the horizontal dispersive term defined in Eq. (37). Note that the emittance increase depends on the product of the x and y beta functions in the quad, and the ratio of the initial x and y emittance values, which may be a very sensitive error for flat beams ($\varepsilon_{x0}/\varepsilon_{y0} \gg 1$) in a linear collider. Since the emittance increase is proportional to the initial emittance (out of plane), these might be described as multiplicative effects (for $\xi^2 \ll 1$). They are also correctable if the correlations remain in tact. This coupling affects the time-sliced emittance, unless $\xi^2 \gg 1$ and the energy spread is chirped, in which case the vertical emittance growth becomes an additive effect equivalent to the angular dispersion error described in Eq. (29).

3.3.3 Sextupole Magnet Transverse Offset

Sextupole magnets are used to correct chromatic focusing errors or linearize bunch compression, etc. Whereas a misaligned quadrupole magnet produces steering and dispersion, a misaligned sextupole magnet can generate all of these, plus x-y coupling and a beta-mismatch error. The vertical field of a normal sextupole magnet [12] is $B_y = \frac{1}{2}K_2(x^2-y^2)p/e$, while the horizontal field is $B_x = -K_2xyp/e$, with K_2 (m^{-3}) related to the second derivative of the transverse field: $K_2 \equiv (\partial^2 B_y/\partial x^2)e/p$, p is the electron momentum, and e is the electron charge. Allowing again for a nominal horizontal dispersion, η, at the sextupole location, and a misalignment in each plane (x_s and y_s), we replace x_0 with $x_0 + \eta\delta - x_s$, and y_0 with $y_0 - y_s$. We can then represent the resulting kick in each plane as

$$\Delta x' = B_y L e/p = \frac{1}{2}K_2 L\left[x_0^2 + 2\eta x_0\delta + \eta^2\delta^2 - y_0^2 - 2x_s x_0 - 2x_s\eta\delta + x_s^2 + 2y_s y_0 - y_s^2\right], \tag{41}$$

$$\Delta y' = B_x L e/p = -K_2 L\left[x_0 y_0 + \eta y_0\delta - y_s x_0 - y_s\eta\delta - x_s y_0 + x_s y_s\right], \tag{42}$$

where L is the sextupole magnet length. We can now ignore all 2nd-order terms (x_0^2, $x_0\delta$, δ^2, y_0^2, $y_0\delta$, and x_0y_0) which are not dependent on alignment and should anyway cancel with the surrounding optics (the whole reason the sextupole magnet is there), and we also ignore constant terms, x_s^2 and y_s^2, which represent simple beam steering, but we keep all linear alignment dependent terms such as: x_sx_0, $x_s\delta$, x_sy_0, y_sy_0, y_sx_0, and $y_s\delta$ and write the remaining, error-driven kicks as

$$\Delta x' = -K_2 L\left[x_s(x_0+\eta\delta) - y_s y_0\right], \tag{43}$$

$$\Delta y' = K_2 L\left[x_s y_0 + y_s(x_0+\eta\delta)\right]. \tag{44}$$

The equivalent emittances in each plane for a misaligned (x_s and y_s) thin sextupole are again calculated using Eq. (28).

$$\frac{\Delta\bar{\varepsilon}_x}{\varepsilon_{x0}} = \frac{1}{2}K_2^2 L^2 \beta_{x0}^2 \left[x_s^2(1+\xi^2) + y_s^2\chi^2\right], \tag{45}$$

$$\frac{\Delta\bar{\varepsilon}_y}{\varepsilon_{y0}} = \frac{1}{2}K_2^2 L^2 \beta_{x0}\beta_{y0}\left(\frac{\varepsilon_{x0}}{\varepsilon_{y0}}\right)\left[x_s^2\chi^2 + y_s^2(1+\xi^2)\right], \tag{46}$$

where the horizontal dispersive term, ξ^2, is defined in Eq. (37), and we also introduce a new parameter, χ^2, which is the square of the ratio of the vertical to horizontal (monochromatic) beam size (*i.e.*, does not include the horizontal dispersive contribution to the horizontal beam size).

$$\chi^2 \equiv \frac{\beta_{y0}\varepsilon_{y0}}{\beta_{x0}\varepsilon_{x0}} \tag{47}$$

The emittance effect is additive if $\xi^2 \gg 1$, and multiplicative if $\xi^2 \ll 1$. Since the misaligned sextupole generates dispersion, x-y coupling, and a beta-mismatch, it is reversible. However, special care should be taken when introducing a sextupole magnet to a beamline. Misalignments will generate correlations in the beam which are not easily corrected downstream unless provisions are made, or the sextupole magnet is adequately aligned.

3.4 Skew Quadrupole Coupling

Cross-plane coupling can be generated by rotated quadrupole magnets or offset sextupoles, so it may be useful to add skew quadrupole magnets to the beamline to allow empirical corrections. To be general, we assume a skew-quad is located at a point in the beamline with nominal horizontal dispersion, η. Like a normal thin-lens quadrupole magnet with an inverse focal length, $1/f_0 = GLe/p$, where G is the field gradient and L is the magnet length, the skew-quad adds cross-plane kicks as $\Delta x' = -y_0/f_0$ and $\Delta y' = (x_0 + \eta\delta)/f_0$. The equivalent emittances in each plane for a skew-quadrupole magnet are again calculated using Eq. (28).

$$\frac{\Delta\bar{\varepsilon}_x}{\varepsilon_{x0}} = \frac{1}{2}\left(\frac{\varepsilon_{y0}}{\varepsilon_{x0}}\right)\frac{\beta_{x0}\beta_{y0}}{f_0^2}, \tag{48}$$

$$\frac{\Delta\bar{\varepsilon}_y}{\varepsilon_{y0}} = \frac{1}{2}\left(\frac{\varepsilon_{x0}}{\varepsilon_{y0}}\right)\frac{\beta_{x0}\beta_{y0}}{f_0^2}\left(1+\xi^2\right), \tag{49}$$

with ξ^2 defined in Eq. (37).

Figure 7 shows an example of vertical emittance correction using a skew-quadrupole magnet located in the LCLS first bunch compressor chicane. The parameters are listed in the caption and Eq. (49) predicts a 14% emittance change going from from $GL = 0$ to $GL = 0.022$ kG, which is quite comparable to the measured change of 15%. And we

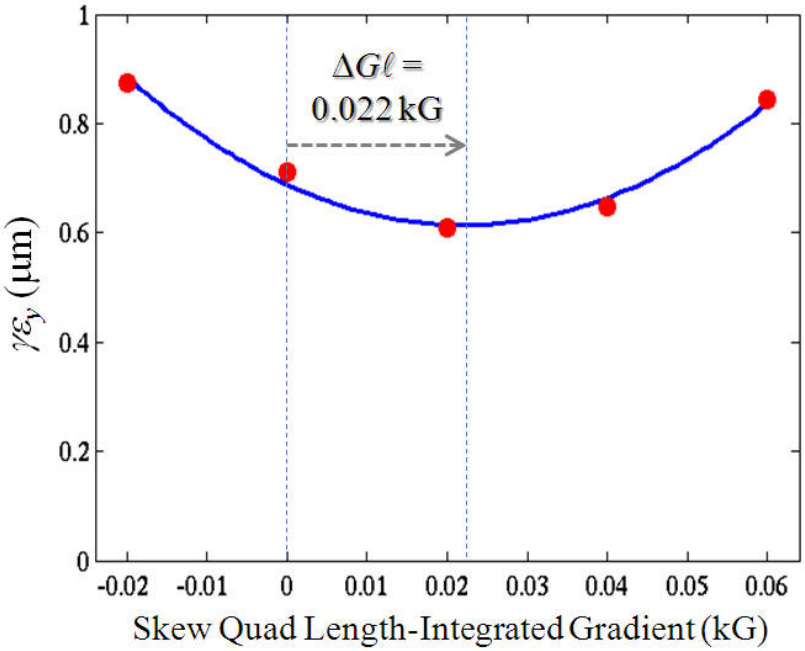

Figure 7: An example vertical (normalized) emittance measurement as a function of skew quadrupole strength. The emittance was reduced by 15% by setting the skew-quad strength (length-integrated field gradient, ΔGL) from zero to 0.022 kG. The beam parameters are: $E \approx 220$ MeV, $\gamma\varepsilon_{x0} \approx \gamma\varepsilon_{y0} \approx 0.6\mu$m, $\beta_{x0} \approx 3$ m, $\beta_{y0} \approx 8$ m, $\eta \approx 180$ mm, $\sigma_\delta \approx 1.2\%$ and $f \approx 330$ m at $GL = 0.022$ kG.

note again here that the equivalent emittance growth is approximately equal the standard emittance growth for a small relative emittance increase. The effect can be quite sensitive for a flat beam ($\varepsilon_{y0}/\varepsilon_{x0} \ll 1$), such as in a linear collider, and the vertical emittance growth may be very sensitive, especially if $\xi^2 \gg 1$. These formulas reduce to those of the rolled quadrupole magnet, Eq. (39) and (40), if $\phi = \pm\pi/4$.

3.5 Magnet Field Quality Errors

Real magnets will include unwanted multipole field errors, such as a weak sextupole field in a dipole magnet (see Fig. 8). These multipoles can introduce chromatic and/or geometric optical aberrations, which can degrade the emittance. We introduce a general multipole field expansion [13] with *normal* and *skew* components, B_n and A_n, as the real and the imaginary parts of the expansion coefficients.

$$B_y + iB_x = \sum_{n=0}^{\infty}(B_n + iA_n)\left(\frac{x+iy}{r_0}\right)^n \tag{50}$$

Here r_0 is a reference radius usually similar to the probe size used to measure the field harmonics (*e.g.*, 2/3 of the bore radius), and n is the harmonic number, where the number of poles is: $2n+2$ ($n = 0$: dipole, $n = 1$: quadrupole, $n = 2$: sextupole, $n = 3$: octupole,

$n = 4$: decapole, and $n = 5$: dodecapole). For example, a weak *normal* sextupole field error (*e.g.*, $n = 2, B_2 \neq 0, A_2 = 0$) in a dipole magnet (typically due to insufficient pole width) can be described using Eq. (50) as $B_y = B_2(x^2 - y^2)/r_0^2$, and we can normalize this sextupole component to the main dipole field, B_0, as a relative error B_2/B_0, typically a small fraction such as 0.1%, depending on the probe radius, r_0, used. We next apply this expansion to some specific cases of multipole errors in standard magnets (quadrupoles and dipoles).

3.5.1 Quadrupole Field Error in a Dipole Magnet

A small quadrupole field component error may arise in a dipole magnet, possibly due to slightly canted pole angles. This field error appears as a simple linear field gradient, $\partial B_y/\partial x \neq 0$, in the bend magnet. We begin by defining the main (vertical) dipole field as B_0, and the fractional quadrupole field content as $|B_1/B_0| \ll 1$ (evaluated at some radius r_0). From Eq. (50) the additional vertical field due to the small *normal* quadrupole component is: $\Delta B_y = B_1 x/r_0$, and the horizontal kicks are $\Delta x' = -\Delta B_y Le/p$, where L is the length of the dipole magnet. We then introduce the dipole's nominal (horizontal) bend angle, $\theta_0 = B_0 Le/p$, and also include the possibility of a nominal dispersion function at the bend, η, resulting in kicks of: $\Delta x' = -\theta_0(B_1/B_0)(x_0 + \eta\delta)/r_0$. The vertical kicks are: $\Delta y' = \theta_0(B_1/B_0)y_0/r_0$, and the equivalent emittance, again using Eq. (28), for each plane for this *normal* quadrupole field component error in a thin dipole magnet is

$$\frac{\Delta\bar{\varepsilon}_x}{\varepsilon_{x0}} = \frac{1}{2}\theta_0^2 \left(\frac{B_1}{B_0}\right)^2 \frac{\beta_{x0}^2}{r_0^2}(1 + \xi^2), \tag{51}$$

$$\frac{\Delta\bar{\varepsilon}_y}{\varepsilon_{y0}} = \frac{1}{2}\theta_0^2 \left(\frac{B_1}{B_0}\right)^2 \frac{\beta_{y0}^2}{r_0^2}, \tag{52}$$

where ξ is defined in Eq. (37).

For strong dipoles with large dispersion and significant energy spread, $\xi^2 \gg 1$, such as a bunch compressor dipole magnet, the tolerable level of quadrupole error can be very demanding. For beam parameters such as in the LCLS second bunch compressor chicane ($E \approx 4.3$ GeV, $\theta_0 \approx 0.035$, $\gamma\varepsilon_{x0} \approx 0.5$ μm, $\beta_{x0} \approx 30$ m, $\eta \approx 360$ mm, $\sigma_\delta \approx 0.5\%$), the horizontal emittance increase is 7% for a quadrupole field error of $|B_1/B_0| = 0.1\%$ measured at $r_0 = 30$ mm. Note that the field error tolerance, $|B_1/B_0|$, doubles in value if the reference radius, r_0, doubles. In order to allow evaluation, the measured field errors must always be accompanied by the relevant probe radius, r_0, used during field measurements. In comparison, the vertical emittance growth is completely insignificant here, $\Delta\bar{\varepsilon}_y/\varepsilon_{y0} < 0.01\%$, since the beam is not dispersed in this direction (*i.e.*, the nominal dispersion, η, is only in the horizontal plane for these examples). Finally, the quantity (B_1/B_0) is typically based on magnetic measurements, but may be less accessible to some, so we also express this quantity in more familiar terms: $(B_1/B_0) = K_1 r_0 L/\theta_0$, where $K_1 \equiv (\partial B_y/\partial x)e/p$, with p as the electron momentum, and e as the electron charge.

3.5.2 Sextupole Field Error in a Dipole Magnet

A small sextupole field error is common in a dipole magnet, possibly due to pole widths which are too small with respect to the typical highly dispersed bend-plane beam size in the magnet (see Fig. 8). From Eq. (50) the additional vertical field due to the small sextupole component is: $\Delta B_y = B_2[(x_0+\eta\delta)^2 - y_0^2]/r_0^2$ and the additional horizontal field is: $\Delta B_x = 2B_2(x_0+\eta\delta)y_0/r_0^2$. The horizontal kicks are $\Delta x' = \Delta B_y Le/p = \theta_0(B_2/B_0)[(x_0+\eta\delta)^2 - y_0^2]/r_0^2$ and the vertical kicks are $\Delta y' = -\Delta B_x Le/p = -2\theta_0(B_2/B_0)(x_0+\eta\delta)y_0/r_0^2$. However, once again, as in the treatment of 2nd-order dispersion (see Eq. (33)), the mean horizontal kick is not zero here: $\langle\Delta x'\rangle = \theta_0(B_2/B_0)(\langle x_0^2\rangle + \eta^2\langle\delta^2\rangle - \langle y_0^2\rangle)/r_0^2$, where $\langle x_0\delta\rangle = 0$ by definition. However, the mean vertical kick is zero if: $\langle x_0 y_0\rangle = 0$ and $\langle y_0\delta\rangle = 0$ (*i.e.*, no initial x-y coupling and no vertical dispersion). To include the non-zero mean, we rewrite Eq. (28) as

$$\frac{\Delta\bar{\varepsilon}_x}{\varepsilon_{x0}} = \frac{\beta_{x0}}{2\varepsilon_{x0}}\left(\langle\Delta x'^2\rangle - \langle\Delta x'\rangle^2\right). \tag{53}$$

The first moment squared and the 2nd-moment of the horizontal kicks are

$$\langle\Delta x'\rangle^2 = \frac{\theta_0^2}{r_0^4}\left(\frac{B_2}{B_0}\right)^2\left[\langle x_0^2\rangle^2 + 2\eta^2\langle x_0^2\rangle\langle\delta^2\rangle - 2\langle x_0^2\rangle\langle y_0^2\rangle - 2\eta^2\langle y_0^2\rangle\langle\delta^2\rangle + \eta^4\langle\delta^2\rangle^2 + \langle y_0^2\rangle^2\right], \tag{54}$$

$$\langle\Delta x'^2\rangle = \frac{\theta_0^2}{r_0^4}\left(\frac{B_2}{B_0}\right)^2\left[\langle x_0^4\rangle + 6\eta^2\langle x_0^2\delta^2\rangle - 2\langle x_0^2 y_0^2\rangle - 2\eta^2\langle y_0^2\delta^2\rangle + \eta^4\langle\delta^4\rangle + \langle y_0^4\rangle\right], \tag{55}$$

where we assume a symmetric distribution such that $\langle x_0^3\delta\rangle = 0$, $\langle x_0\delta^3\rangle = 0$, and $\langle x_0 y_0^2\delta\rangle = 0$. Next we separate the uncorrelated variables such that $\langle x_0^2\delta^2\rangle = \langle x_0^2\rangle\langle\delta^2\rangle$, $\langle x_0^2 y_0^2\rangle = \langle x_0^2\rangle\langle y_0^2\rangle$ and take the difference,

$$\begin{aligned}&\langle\Delta x'^2\rangle - \langle\Delta x_0'\rangle^2 = \\ &\frac{\theta_0^2}{r_0^4}\left(\frac{B_2}{B_0}\right)^2\left[\langle x_0^4\rangle - \langle x_0^2\rangle^2 + 4\eta^2\langle x_0^2\rangle\langle\delta^2\rangle + \eta^4\left(\langle\delta^4\rangle - \langle\delta^2\rangle^2\right) + \langle y_0^4\rangle - \langle y_0^2\rangle^2\right].\end{aligned} \tag{56}$$

We also assume all Gaussian distributions where $\langle x_0^4\rangle = 3\langle x_0^2\rangle^2$, $\langle y_0^4\rangle = 3\langle y_0^2\rangle^2$, and $\langle\delta^4\rangle = 3\langle\delta^2\rangle^2$ and the equivalent emittance in each plane, now using Eq. (53), for this *normal* sextupole field component error in a thin dipole magnet is

$$\frac{\Delta\bar{\varepsilon}_x}{\varepsilon_{x0}} = \theta_0^2\left(\frac{B_2}{B_0}\right)^2\frac{\beta_{x0}^3\varepsilon_{x0}}{r_0^4}\left[\left(1+\xi^2\right)^2 + \chi^4\right], \tag{57}$$

$$\frac{\Delta\bar{\varepsilon}_y}{\varepsilon_{y0}} = 2\theta_0^2\left(\frac{B_2}{B_0}\right)^2\frac{\beta_{y0}^2\beta_{x0}\varepsilon_{x0}}{r_0^4}\left(1+\xi^2\right). \tag{58}$$

Here ξ^2 and χ^2 are defined in Eq. (37) and (47), we assume Gaussian distributions in x, y, and δ, and no initial coupling or vertical dispersion, $\langle x_0 y_0\rangle = 0$ and $\langle y_0\delta\rangle = 0$.

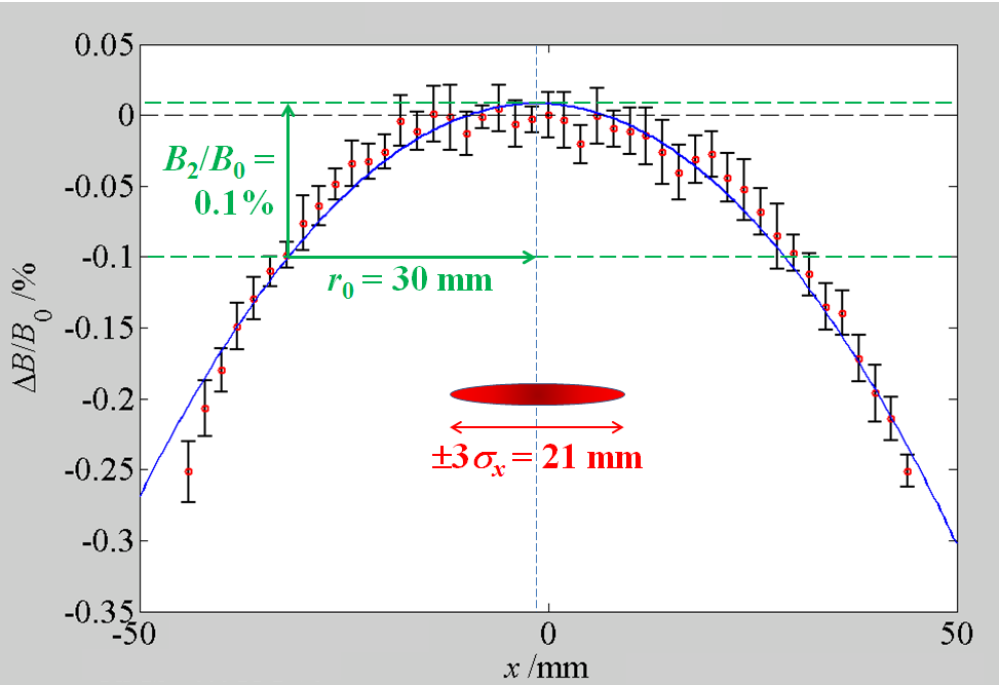

Figure 8: Relative field error in LCLS BC2 dipole magnet measured over horizontal position, x, showing a field error of $B_2/B_0 = -0.1\%$ at $r_0 = 30$ mm. With the beam parameters described above, this sextupole field error should only generate a 2% bend-plane emittance increase for this one magnet. The horizontal rms beam size in the magnet, $\sigma_x = \sqrt{\beta_{x0}\varepsilon_{x0}(1+\xi^2)}$, is indicated out to $\pm 3\sigma_x$.

For beam parameters such as in the LCLS second bunch compressor chicane ($E \approx 4.3$ GeV, $\theta_0 \approx 0.035$, $\gamma\varepsilon_{x0} = \gamma\varepsilon_{y0} \approx 0.5$ μm, $\beta_{x0} \approx 30$ m, $\beta_{y0} \approx 16$ m, $\eta \approx 360$ mm, $\sigma_\delta \approx 0.5\%$), the horizontal emittance increase is 2% for a sextupole field error of $|B_2/B_0| = 0.1\%$ measured at $r_0 = 30$ mm (see Fig. 8). The vertical emittance growth is completely insignificant ($< 0.001\%$) since the beam is not dispersed vertically. Finally, the quantity (B_2/B_0) is typically based on magnetic measurements, but may be less accessible to some, so we also express this quantity in more familiar terms: $(B_2/B_0) = \frac{1}{2}K_2 r_0^2 L/\theta_0$, where $K_2 \equiv (\partial^2 B_y/\partial x^2)e/p$, with p as the electron momentum, and e the electron charge.

3.6 Chromaticity of a Quadrupole Magnet

The focal length, f, of a quadrupole magnet is dependent on the electron relative energy deviation, $|\delta| \ll 1$. The kicks from a thin-lens quadrupole magnet with significant energy spread are

$$\Delta x' = \frac{x_0}{f_0(1+\delta)} \approx \frac{x_0(1-\delta)}{f_0}, \tag{59}$$

where f_0 is the focal length at $\delta = 0$. We can ignore the x_0/f_0 term here as the nominal focusing, and instead concentrate on the energy dependent error: $\Delta x' = -(x_0 + \eta\delta)\delta/f_0$,

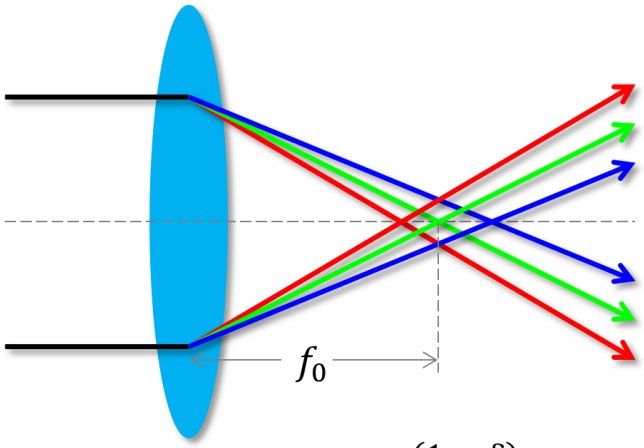

Figure 9: The focal length, f, of a quadrupole magnet is dependent on the relative energy deviation, δ, indicated here as color variations.

where we have replaced x_0 with $x_0 + \eta\delta$ to include a possible nominal (horizontal) dispersion at the quadrupole. The vertical kicks are of the same form but with $\eta = 0$. We also note that this 2nd-order effect (chromatic aberration) generates a non-zero mean value of the kicks: $\langle \Delta x' \rangle = -\eta \langle \delta^2 \rangle / f_0$, and we need to use the equivalent emittance form of Eq. (53) with the result

$$\frac{\Delta\bar{\varepsilon}_x}{\varepsilon_{x0}} = \frac{1}{2}\frac{\beta_{x0}^2}{f_0^2}\left(1 + 2\xi^2\right)\sigma_\delta^2, \tag{60}$$

$$\frac{\Delta\bar{\varepsilon}_y}{\varepsilon_{y0}} = \frac{1}{2}\frac{\beta_{y0}^2}{f_0^2}\sigma_\delta^2. \tag{61}$$

The factor of 2 in the second term of Eq. (60) is based on a Gaussian energy distribution where the fourth moment is related to the square of its second moment as $\langle \delta^4 \rangle = 3\sigma_\delta^4$, as used previously. Note that this factor of 2 is replaced by 4/5 for a uniform distribution. This chromatic evaluation is useful in determining if the quadrupole magnet setting is too strong with respect to the rms energy spread (σ_δ), dispersion, and beta function at that location (*e.g.*, if $\Delta\bar{\varepsilon}/\varepsilon_0 > 2\%$). The chromatic aberration can be corrected with sextupole magnets at dispersive locations (*e.g.*, a 2nd-order achromat [14]) or with more quadrupole magnets and appropriate placement and strength. Note that we have assumed a thin-lens magnet here which may be somewhat inaccurate for very strong focusing, for example with focal length less than or similar to magnet length.

3.7 Sextupole Abberations

A sextupole magnet may be added to a beamline to generate non-linear bunch compression terms, such as T_{566}. In this case, the bunch compression can be linearized, but the

sextupole, even if aligned perfectly, will generate transverse geometric, chromatic, and 2nd-order dispersive aberrations. These can quickly dilute the transverse emittance levels depending on the beta and dispersion functions in the sextupole magnet. As shown above, the vertical sextupole field can be described as $B_y = \frac{1}{2}K_2(x^2 - y^2)p/e$, while the horizontal field is $B_x = -K_2xyp/e$, with K_2 related to the second derivative of the transverse field: $K_2 \equiv (\partial^2 B_y/\partial x^2)e/p$. The horizontal kicks are $\Delta x' = \frac{1}{2}K_2L\left[(x_0 + \eta\delta)^2 - y_0^2\right]$ and the vertical are $\Delta y' = K_2L\,(x_0 + \eta\delta)\,y_0$. We see that $\langle\Delta x'\rangle \neq 0$, and so need to include this, although $\langle\Delta y'\rangle = 0$. Then using Eq. (53) to find the equivalent emittance growth for both planes

$$\frac{\Delta\bar{\varepsilon}_x}{\varepsilon_{x0}} = \frac{1}{4}K_2^2L^2\beta_{x0}^3\varepsilon_{x0}\left[\left(1+\xi^2\right)^2 + \chi^4\right], \tag{62}$$

$$\frac{\Delta\bar{\varepsilon}_y}{\varepsilon_{y0}} = \frac{1}{2}K_2^2L^2\beta_{x0}\beta_{y0}^2\varepsilon_{x0}\left(1+\xi^2\right). \tag{63}$$

This is the relative equivalent emittance growth generated by one well aligned sextupole magnet located in a horizontal dispersion region and with a significant energy spread. A sextupole magnet with $K_2 = 0.5$ m^{-3}, length $L = 0.1$ m, and with $\beta_{x0} = 12.6$ m, $\beta_{y0} = 11.3$ m, $\eta = 520$ mm, $\sigma_\delta = 1\%$, and $\varepsilon_{N_0} = 0.5$ μm, produces a horizontal relative equivalent emittance growth of 10%, but no significant growth in the vertical plane.

3.8 Coulomb Scattering

A thin foil in the beam path may be useful for vacuum isolation or for beam size diagnostics but the Coulomb scattering of the electrons through the foil material can also degrade the emittance and generate a mismatch (by adding angular spread to the beam). A thin slotted foil can also be used to generate a femtosecond or sub-femtosecond x-ray pulse in an FEL [15]. The rms angular spread generated by a beam with energy, E, is

$$\langle\Delta x'^2\rangle^{1/2} \approx \frac{E_0}{E}\sqrt{\frac{L}{L_0}}\left(1 + \frac{1}{9}\log_{10}\left(\frac{L}{L_0}\right)\right) \tag{64}$$

where $E_0 \approx 14$ MeV, L is the thickness of the foil, and L_0 is the radiation length of the foil material. The equivalent emittance using Eq. (28) is

$$\frac{\Delta\bar{\varepsilon}}{\varepsilon_0} \approx \frac{1}{2}\frac{\beta_0}{\varepsilon_0}\frac{E_0^2}{E^2}\frac{L}{L_0}\left(1 + \frac{1}{9}\log_{10}\left(\frac{L}{L_0}\right)\right)^2, \tag{65}$$

representing either x or y as needed. For LCLS BC2 beam parameters at chicane center, $E = 4.3$ GeV, $\beta_0 = 20$ m, $\gamma\varepsilon_0 = 0.5$ μm, and a 3-μm thick Al foil ($L_0 = 8.9$ cm), the emittance increases by about a factor of 10. Note that Eq. (64) is only accurate within $0.001 < L/L_0 < 1000$, although not a large error in our case here. This effect is not correctable since the angular scattering is a stochastic process and is not correlated with any coordinate within the bunch. Figure 10 shows the measured beam size increase with a 3-μm thick Al foil roughly consistent with the factor of 10 emittance increase.

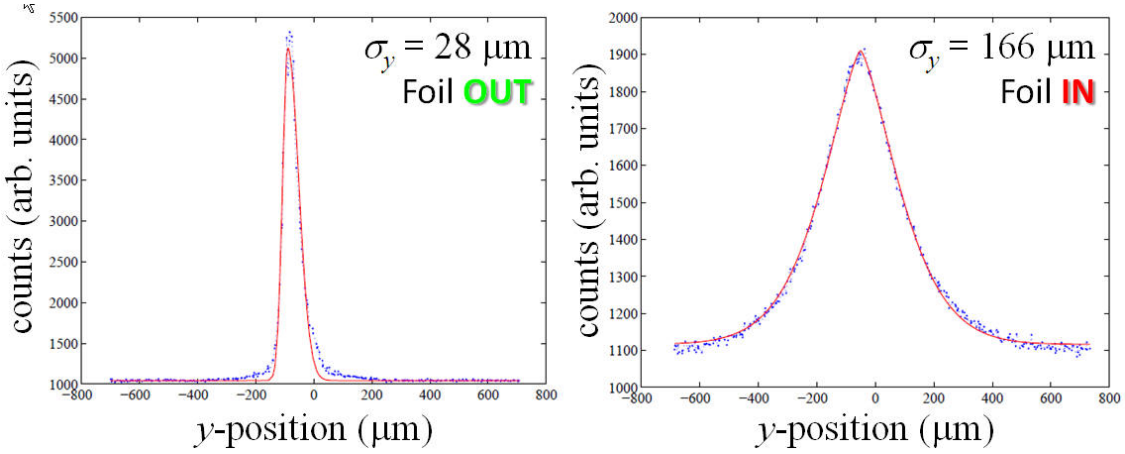

Figure 10: Measured coulomb scattering through a 3-μm thick Al foil located in the LCLS 2nd bunch compressor. The rms vertical beam size downstream of the compressor is 28 μm at left (foil extracted) and 166 μm at right (foil inserted).

3.9 Incoherent Synchrotron Radiation

Synchrotron radiation is emitted by high-energy electrons as they are bent through a dipole magnet, generating an additional random energy spread. After emission, electrons with lower energy will be over-bent, resulting in a dilution of the bend-plane emittance after the dipole magnet. The rms relative energy spread induced by ISR (incoherent synchrotron radiation, where the bunch length is much longer than wavelengths which propagate in the vacuum chamber) generated over a bend magnet of length L and bend radius ρ is [16]

$$\sigma_\delta^2 = \frac{55}{24\sqrt{3}} \frac{r_e \hbar c}{(mc^2)^6} \frac{E^5 L}{|\rho^3|}, \tag{66}$$

where r_e is the classical electron radius, mc^2 is the electron rest mass, $\hbar$ is Planck's constant divided by 2π, and E is the electron energy. For a given electron energy and small bend angle ($\theta_0 = L/\rho$), a longer bend magnet will reduce the effect (seen by replacing ρ in Eq. (66) with L/θ_0).

For incoherent radiation (*i.e.*, δ is random with no correlation to other local phase space coordinates), we calculate the variance of Δx, $\Delta x'$, and their product evaluated at a downstream location s_0 (just after the bend) and due to the energy spread generated at each upstream beamline location $s < s_0$, and we sum these in quadrature over the beamline as uncorrelated quantities [17],

$$\langle \Delta x^2 \rangle = \int_0^{s_0} R_{16}^2(s) \frac{d}{ds} \sigma_\delta^2 ds, \tag{67}$$

$$\langle \Delta x'^2 \rangle = \int_0^{s_0} R_{26}^2(s) \frac{d}{ds} \sigma_\delta^2 ds, \tag{68}$$

$$\langle \Delta x \Delta x' \rangle = \int_0^{s_0} R_{16}(s) R_{26}(s) \frac{d}{ds} \sigma_\delta^2 ds. \tag{69}$$

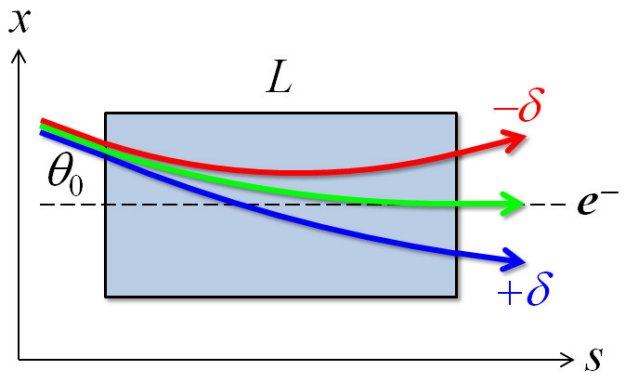

Figure 11: The final dipole magnet of an arbitrary bend system typically terminates the dispersion function to zero at its exit. However, electrons which change energy just upstream of, or inside the bend, rather than upstream of the entire bend system, will follow a different bend-plane trajectory as shown, where the green trajectory is the on-energy path.

Here R_{16} is the linear transfer matrix element (dispersion) which maps a small relative energy deviation, δ, originating at s, onto a horizontal position change, Δx, observed at s_0, while R_{26} similarly maps δ onto $\Delta x'$. Here we no longer have 'point-like' scattering since we are integrating contributions over the beam line rather than just one thin component. The square of the incrementally generated energy spread is represented here by its rate of change along the beamline ($d\sigma_\delta^2/ds$). For a bend magnet with constant bend radius (typical) the rate of increase of the energy spread squared is also constant, as seen in Eq. (66), by replacing L with s, and so the rate can be removed from the integrals of Eqs. (67), (68), and (69).

The task of calculating the effect on the equivalent emittance now requires evaluation of these integrals, but first we need to express R_{16} and R_{26} as functions of s, L, and ρ, which depend on the particular layout of the bend system. For a simple case we take just the final dipole magnet of a bend system (*e.g.*, last bend of a symmetric 4-dipole magnetic chicane), where the dispersion function terminates to zero at its exit, as shown in Fig. 11.

In this case the transfer matrix elements are: $R_{16}(s) = -\frac{s^2}{2\rho}$ and $R_{26}(s) = -\frac{s}{\rho}$, and the variance values in Eqs. (67), (68), and (69), integrated over the bend magnet length, are:

$$\langle \Delta x^2 \rangle = \frac{d\sigma_\delta^2}{ds} \int_{-L}^{0} \frac{s^4}{4\rho^2} ds = \frac{d\sigma_\delta^2}{ds} \frac{L^5}{20\rho^2}, \tag{70}$$

$$\langle \Delta x'^2 \rangle = \frac{d\sigma_\delta^2}{ds} \int_{-L}^{0} \frac{s^2}{\rho^2} ds = \frac{d\sigma_\delta^2}{ds} \frac{L^3}{3\rho^2}, \tag{71}$$

$$\langle \Delta x \Delta x' \rangle = \frac{d\sigma_\delta^2}{ds} \int_{-L}^{0} \frac{s^3}{2\rho^2} ds = \frac{d\sigma_\delta^2}{ds} \frac{L^4}{8\rho^2}. \tag{72}$$

Note that $\langle \Delta x \Delta x' \rangle^2 \approx \langle \Delta x^2 \rangle \langle \Delta x'^2 \rangle$ and this nearly 'point-like' scattering case is close to that of Eq. (11) with almost no additive emittance. Inserting these into Eq. (22) gives the

relative equivalent emittance growth due to ISR for only the final dipole magnet of a bend system.

$$\frac{\Delta\bar{\varepsilon}}{\varepsilon_0} = \frac{55}{48\sqrt{3}}\frac{r_e\hbar c}{(mc^2)^7}\frac{E^6|\theta_0^5|}{\varepsilon_{N_0}L^2}\left(\frac{\beta_0}{3}+\frac{\alpha_0 L}{4}+\frac{\gamma_0 L^2}{20}\right) \tag{73}$$

Here $\varepsilon_{N_0} = \gamma\varepsilon_0$ is the initial normalized emittance, and $d\sigma_\delta^2/ds$ is taken from Eq. (66) with s substituted for L and then differentiated with respect to s, and we have replaced ρ with L/θ_0. Note that γ_0 here is the Twiss parameter, $\gamma_0 \equiv (1+\alpha_0^2)/\beta_0$, with β_0 and α_0 evaluated at the exit of the bend.

Equation (73) is for ISR in one bend only, but shows the sensitivity to electron energy (E^6), bend angle ($|\theta_0^5|$), and bend magnet length. Long bends will reduce the emittance growth, but the final term in parenthesis ($\gamma_0 L^2/20$) suggests a limit to this direction, depending on the Twiss parameters immediately after the bend. An optimum might be derived, but with only one bend included here it is not a meaningful exercise. The case of a full 4-dipole chicane is calculated below. Finally, it is important to recognize that ISR is not error driven. It is an issue that must be handled in the optics design and cautions the use of large bend angles at high energy.

For parameters of the LCLS BC2 compressor (set to its maximum strength) with $E = 4.3$ GeV, $\beta_0 = 5$ m, $\alpha_0 = -0.5$, $\varepsilon_{N_0} = 0.5$ μm, $L = 0.54$ m, $|\theta_0| = 35$ mrad, the relative equivalent emittance increase is about 0.015%.

For completion, we also present here the ISR results for an entire 4-dipole chicane, with L_T as the total length of the chicane, ΔL as the edge-to-edge spacing of the first two (and last two) bends, and using Λ^2 as defined below. The second moments of the electron positions and angles immediately after the chicane are based on the R_{16} and R_{26} integrals over all four bends and are given as:

$$\langle\Delta x^2\rangle = \frac{d\sigma_\delta^2}{ds}\int R_{16}^2(s)ds = \frac{L^3\Lambda^2}{30\rho^2}, \tag{74}$$

$$\langle\Delta x'^2\rangle = \frac{d\sigma_\delta^2}{ds}\int R_{26}^2(s)ds = \frac{4L^3}{3\rho^2}, \tag{75}$$

$$\langle\Delta x\Delta x'\rangle = \frac{d\sigma_\delta^2}{ds}\int R_{16}(s)R_{26}(s)ds = \frac{2L_T L^3}{3\rho^2}, \tag{76}$$

with the definition

$$\Lambda^2 \equiv 10L_T(\Delta L - L) + 25\Delta L L + 16L^2 + 20L_T^2 + 20\Delta L^2. \tag{77}$$

The equivalent relative emittance growth due to ISR in all four bends of a chicane , substituting Eqs. (74), (75), and (76) into Eq. (22), is:

$$\frac{\Delta\bar{\varepsilon}}{\varepsilon_0} = \frac{55}{144\sqrt{3}}\frac{r_e\hbar c}{(mc^2)^7}\frac{E^6|\theta_0^5|}{\varepsilon_{N_0}L^2}\left(4\beta_0 + 4\alpha_0 L_T + \gamma_0\frac{\Lambda^2}{10}\right), \tag{78}$$

Note again that $\gamma_0 \equiv (1+\alpha_0^2)/\beta_0$, with β_0 and α_0 evaluated at the exit of the chicane. Using the LCLS BC2 chicane parameters described above, and including the full chicane length, $L_T = 22.4$ m, and each of two drift lengths, $\Delta L = 10$ m, the relative equivalent emittance increase over the full chicane is about 1.0%, which would scale up to 7% at 6 GeV. The rms relative energy spread induced by ISR in the full chicane at 4.3 GeV is only 6×10^{-6}.

3.10 Coherent Synchrotron Radiation

The synchrotron radiation from a bend magnet can be coherent if the electron bunch length is short compared to the longest wavelengths which can propagate in the vacuum chamber. With respect to incoherent radiation where the power scales as N, the coherent radiation power scales by N^2, where N is the number of electrons in the bunch. The high-power radiation from the tail of the bunch can catch up to the head of the bunch as it cuts across the cord of the curved (bending) trajectory and can alter the energy of the various temporal slices of the bunch as it passes through the bend, ultimately steering each slice differently after the bend, and diluting the bend-plane emittance [21].

The approximate rms relative energy spread induced by CSR (coherent synchrotron radiation) generated over a bend magnet of length L and bend radius ρ (assuming a Gaussian temporal bunch profile and steady-state conditions) is [18]

$$\sigma_\delta \approx 0.22 \frac{r_e mc^2 NL}{E\rho^{2/3}\sigma_z^{4/3}}, \tag{79}$$

where r_e is the classical electron radius, E is the electron energy, and σ_z is the rms bunch length in the bend (assumed constant here). Again we can define the rate of energy spread increase using Eq. (79), substituting s for L, and differentiating with respect to s. In this case (*i.e.*, CSR) the energy spread increases linearly with distance, s, whereas with ISR the *square* of the energy spread increases linearly with distance (see Eq. (66)).

For this CSR wakefield effect, where a particle's energy deviation at the end of the bend system is purely a function of its longitudinal position along the bunch, z, the transverse coordinate shifts, $\Delta x(z)$, which are observed at the end of the bend but originate at each location, s, add linearly, so we first sum $\Delta x(z)$ over the bend length and then find its total variance.

$$\langle \Delta x^2 \rangle = \left(\int_{-L}^{0} R_{16}(s) \frac{d\sigma_\delta}{ds} ds \right)^2 \tag{80}$$

$$\langle \Delta x'^2 \rangle = \left(\int_{-L}^{0} R_{26}(s) \frac{d\sigma_\delta}{ds} ds \right)^2 \tag{81}$$

Due to the coherence and steady-state assumption, the correlation $\langle \Delta x \Delta x' \rangle^2 = \langle \Delta x^2 \rangle \langle \Delta x'^2 \rangle$, and we have the 'point-like' kicks of Eq. (11). The difference between the incoherent and the coherent process is now clear as the ISR integrals in Eqs. (67), (68), and (69), represent a monotonically increasing summation of positive values, whereas the CSR integrals of Eqs. (80) and (81), are a summation of signed quantities which might be made to vanish [17].

Again, for a dipole magnet with constant bend radius and assuming the bunch length does not change in this last bend magnet (typical in bunch compressor chicanes), the rate of increase of the energy spread is then constant, as seen in Eq. (79), by replacing L with s. So once again the rate can be removed from the integral here. Evaluating the equivalent emittance again requires substituting Eqs. (80) and (81) into Eq. (23) with $\langle \Delta x \Delta x' \rangle^2 = \langle \Delta x^2 \rangle \langle \Delta x'^2 \rangle$, and the transfer matrix elements again are: $R_{16}(s) = -\frac{s^2}{2\rho}$ and

$R_{26}(s) = \frac{s}{\rho}$ over the final dipole magnet of a bend system, as shown in Fig. 11.

$$\langle \Delta x^2 \rangle = \left(\frac{d\sigma_\delta}{ds} \int_{-L}^{0} \frac{s^2}{2\rho} ds \right)^2 = \left(\frac{d\sigma_\delta}{ds} \right)^2 \frac{L^6}{36\rho^2} \tag{82}$$

$$\langle \Delta x'^2 \rangle = \left(\frac{d\sigma_\delta}{ds} \int_{-L}^{0} \frac{s}{\rho} ds \right)^2 = \left(\frac{d\sigma_\delta}{ds} \right)^2 \frac{L^4}{4\rho^2} \tag{83}$$

Inserting these into Eq. (23) gives the approximate relative equivalent emittance growth due to CSR for the final dipole in a bend system assuming a Gaussian temporal bunch profile and steady-state conditions (ignores possible vacuum chamber shielding and any transient effects at the start of the bend).

$$\frac{\Delta\bar{\varepsilon}}{\varepsilon_0} \approx 0.024 \frac{r_e^2 N^2}{\varepsilon_{N_0}} \frac{mc^2}{E} \left(\frac{L|\theta_0^5|}{\sigma_z^4} \right)^{2/3} \left(\frac{\beta_0}{4} + \frac{\alpha_0 L}{6} + \frac{\gamma_0 L^2}{36} \right) \tag{84}$$

Here $\varepsilon_{N_0} = \gamma\varepsilon_0$ is the initial normalized emittance, and $d\sigma_\delta/ds$ is taken from Eq. (79) with s substituted for L and then differentiated with respect to s.

For parameters of the LCLS BC2 compressor (set to its maximum strength) with $E = 4.3$ GeV, $\beta_0 = 20$ m, $\alpha_0 = -0.81$, $\varepsilon_{N_0} = 0.5$ μm, $L = 0.54$ m, $|\theta_0| = 50$ mrad ($\rho = 10.8$ m), $\sigma_z = 10$ μm, and $N = 1.6 \times 10^9$, the relative equivalent emittance increase is about 40%. For a 3-4 dipole bunch compressor chicane this is an underestimate since it ignores the radiation occurring at the end of the 2nd-to-last bend where the bunch length can be nearly as short as in the last bend, and it also ignores the CSR interaction of the electron bunch in the drift between the last two bends. These effects are better suited to detailed computer tracking, but the scaling is clear in Eq. (84). Finally, a comparison is shown in Fig. 12 as a function of the rms bunch length in the final bend of the chicane. The plot includes particle tracking done with the computer code *Elegant* [19] and is compared to the analytical results of Eq. (84) all under the same parameters and assumptions (final bend only, steady-state conditions, and a Gaussian temporal bunch profile).

3.11 Energy Modulator

Many FEL machine designs require a laser heater system to damp the micro-bunching instability by adding a small intrinsic energy spread to the beam [20]. In such a system, the electron bunch is energy-modulated at optical wavelengths by interacting the electron beam with an optical laser in a short undulator enclosed is a small magnetic chicane. The chicane introduces a transverse offset to the undulator axis (see η in Fig. 13) allowing more convenient injection of the laser into the undulator in order to interact with the electron bunch. The interaction generates an additional energy spread on the electron beam inside the chicane which can also dilute the bend-plane emittance if the system optics are not designed well, much like ISR or CSR.

The energy modulation accumulates over the undulator, as intended, but the off-energy electrons will be bent differently by the last two dipoles of the chicane. Once again we

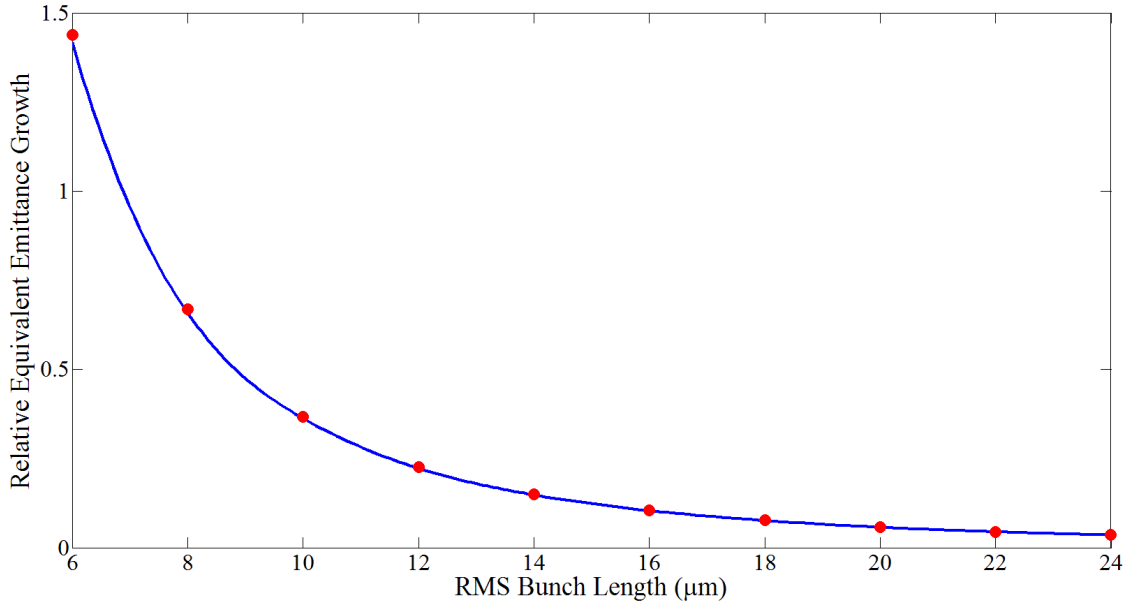

Figure 12: The CSR-induced equivalent relative emittance growth from Eq. (84) (solid-blue) and the same from computer tracking in *Elegant* [19] (red-circles) with steady-state conditions, including the final bend only, and using a Gaussian temporal profile, as assumed in the derivation of Eq. (84).

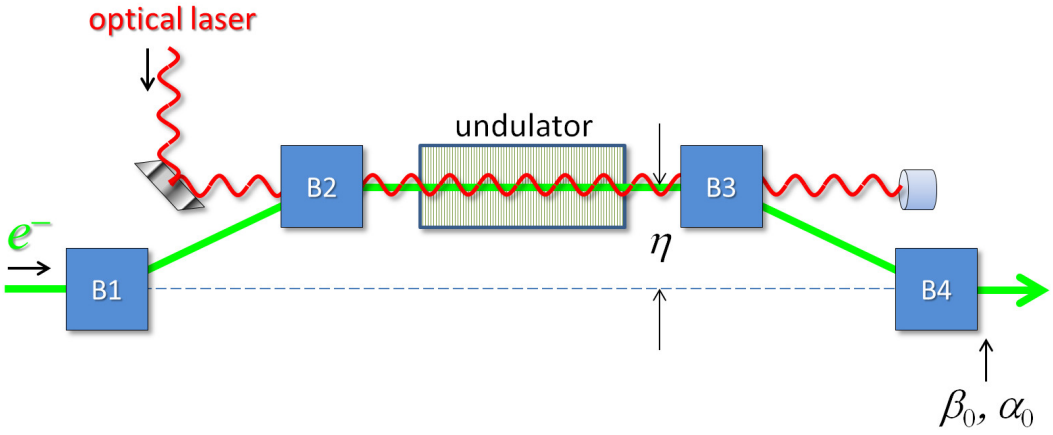

Figure 13: Laser heater arrangement with optical laser interacting in a short undulator enclosed in a 4-bend chicane. The bend-plane offset, η, is provided by the chicane and allows easier laser injection as shown.

need the transfer matrix element, $R_{16} = \eta$, which maps a small relative energy deviation, δ, generated within the undulator, to a position change at the end of the chicane, $\Delta x = R_{16}\delta$. The symmetry of the chicane, as shown in Fig. 13, results in $R_{26} = 0$, so the second moment of the kicked particle positions in the bend-plane immediately after the chicane is

$$\langle \Delta x^2 \rangle = R_{16}^2 \sigma_\delta^2 = \eta^2 \sigma_\delta^2, \tag{85}$$

where η is the bend-plane chicane offset shown in Fig. 13 and σ_δ is the rms relative energy spread (rms modulation) added by the laser interaction.

Substituting $\langle \Delta x^2 \rangle$ into Eq. (22), and with $\langle \Delta x'^2 \rangle = 0$ and $\langle \Delta x \Delta x' \rangle = 0$ (*i.e.*, $R_{26} = 0$), then describes the equivalent bend-plane emittance growth for a laser heater in a chicane.

$$\frac{\Delta \bar{\varepsilon}}{\varepsilon_0} = \frac{1}{2}\left(1 + \alpha_0^2\right) \frac{\eta^2}{\varepsilon_0 \beta_0} \sigma_\delta^2 \tag{86}$$

Here the Twiss parameters β_0 and α_0 are evaluated at the exit of the chicane, and α_0 appears since this is the equivalent emittance growth, which includes the induced matching error.

Using the LCLS laser heater parameters [20], and at the full (extreme) IR-laser pulse energy of 250 μJ, the rms relative (modulated) energy spread generated at 135 MeV is $\sigma_\delta \approx 9 \times 10^{-4}$. With the chicane's bend-plane offset at $\eta = 35$ mm, and Twiss parameters at the end of the last dipole of $\beta_0 = 11$ m and $\alpha_0 = 0.48$, the relative equivalent emittance growth is small at 2.9% for an initial bend-plane emittance of $\varepsilon_{N_0} = 0.5$ μm. With the laser pulse energy set to its nominal value of 45 μJ ($\sigma_\delta < 3.3 \times 10^{-4}$) the calculated emittance growth in Eq. (86) is $< 0.4\%$. Figure 14 (taken from Ref. [20]) shows actual time-sliced emittance measurements at LCLS immediately after the laser heater system. The emittance results are almost unchanged by increasing the laser pulse energy from 45 to 250 μJ, which corresponds to an rms relative energy spread range of 3.3×10^{-4} to 9×10^{-4}. (Note that the generated energy spread scales with the square root of the laser pulse energy.) These emittance measurements are consistent with Eq. (86), which predicts an emittance increase of 0.4% to 2.9% over this range, but these small levels are not resolved in Fig. 14. (Note that the emittance measurements with the laser heater switched off are believed to be underestimated due to coherent radiation generated as the bunch pases through the beam screen which is used to measure the emittance. With the heater turned on, this coherent radiation is suppressed by the larger energy spread and the emittance measurements become more accurate.) It is important to note the value of β_0 here. A much smaller choice can inflate the emittance growth.

3.12 Transverse Wakefields

The electron bunch will interact with a misaligned RF accelerating structure generating a short-range transverse wakefield, where the field established by the leading particles in the bunch at z' (coordinate along the bunch length) kicks the trailing particles at z (negative z toward the bunch head). The transverse kicks, for any particular value of z, are summed over the leading particles and expressed by the convolution integral [22]

$$\Delta x'(z) = -\frac{Ne^2 L}{E} \int_{-\infty}^{z} x(z') f(z') W_x\left(z - z'\right) dz', \tag{87}$$

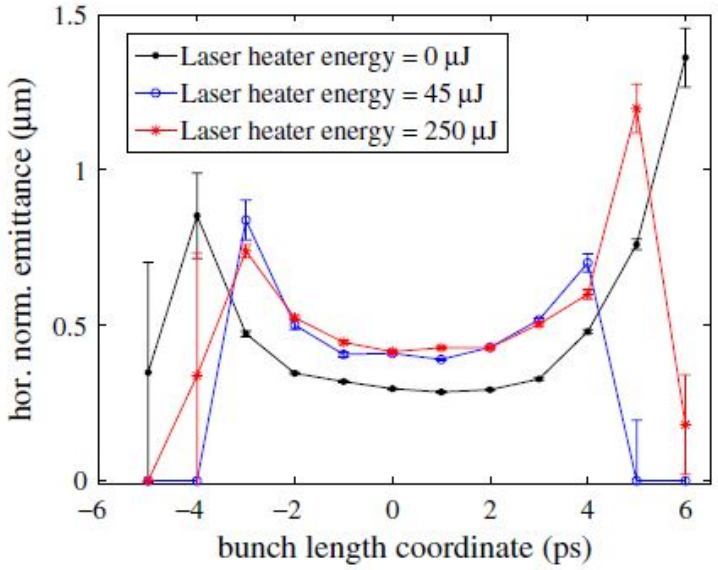

Figure 14: Measured bend-plane time-sliced emittance after the LCLS laser heater and for various settings of the laser pulse energy. The measured emittance growth is insignificant and consistent with Eq. (86). The curve taken with laser heater off is presumed to be an underestimate due to the effects of coherent radiation from the screen (see text).

where $f(z')$ is the temporal bunch distribution normalized to unity, N is the bunch population, L is the structure length, E is the electron energy, $x(z')$ is the transverse offset of the field-generating bunch slice, and W_x is the transverse point-charge dipole wakefield of the RF structure, typically calculated for a precise structure geometry by using an electro-magnetic computer code. The point-charge wake is usually expressed in volts per meter of structure length, per pC of bunch charge, and per millimeter of transverse offset.

The dipole point-charge wake function can be approximated by [22]

$$W_x(z) \approx \frac{4Z_0 c s_1}{\pi a^4}\left[1-(1+\sqrt{z/s_1})e^{-\sqrt{z/s_1}}\right], \tag{88}$$

where a is the mean iris radius over the RF structure, Z_0 is the free-space impedance, and s_1 is the characteristic length of the wake function related to the specific RF structure geometry ($s_1 \approx 0.4$ mm for the NLC X-band structure applied here).

For simplicity, and to allow a closed form solution which indicates the emittance scaling, we will approximate Eq. (88) as a linear function in z (see Fig. 15), and also use a uniform temporal bunch distribution with full length Δz (bunch head at $z = -\Delta z/2$ and bunch tail at $z = \Delta z/2$).

$$W_x(z) \approx \frac{2Z_0 c}{\pi a^4 g}\left(z+\frac{\Delta z}{2}\right) \tag{89}$$

Here we introduce an approximate scaling factor $g \approx 2.5$ in order to best fit the point-charge wake function over the 2.5-mm span of Fig. 15 to a line. This is quite rough but allows an estimate and shows the parameter scaling. More detailed wakefield calculations are better

left to computer codes and particle tracking. Note for $g = 1$ (dotted steepest line of Fig. 15) the linear slope of Eq. (89) is the asymptotic slope for all transverse wakefields evaluated at $z - z' = 0$ and in steady-state conditions.

To estimate the wakefield effect on the electron bunch we take a short accelerating structure ($L \ll \beta_0$) with a transverse misalignment x_0 (constant along z and over L), and in this simplified case Eq. (87) becomes

$$\Delta x'(z) \approx -\frac{2Z_0 cNe^2 Lx_0}{\pi g E a^4 \Delta z} \int_{-\frac{\Delta z}{2}}^{\frac{\Delta z}{2}} \left(z + \frac{\Delta z}{2} - z' \right) dz' = -\frac{2Z_0 cNe^2 Lx_0}{\pi g E a^4} \left(z + \frac{\Delta z}{2} \right), \qquad (90)$$

which shows, for this approximation, that the kicks are a linear function of z along the bunch length, with the bunch head ($z = -\Delta z/2$) not kicked, and the bunch tail ($z = \Delta z/2$) kicked maximum. With this choice of coordinates the mean of z is zero ($\langle z \rangle = 0$), but we have a non-zero mean value of the kicks ($\langle \Delta x' \rangle \neq 0$). Therefore we need to use Eq. (53), rather than Eq. (28), and we find the approximate equivalent emittance growth for a short RF structure with length L, iris radius a, and transverse misalignment x_0 is

$$\frac{\Delta \bar{\varepsilon}}{\varepsilon_0} \approx \frac{2\beta_0}{\varepsilon_0} \left(\frac{Z_0 cNe^2 Lx_0}{\pi g E a^4} \right)^2 \sigma_z^2, \qquad (91)$$

where $\sigma_z = \Delta z/\sqrt{12}$ is the rms bunch length and $g \approx 2.5$ is a rough scaling factor used to approximate this particular point-charge wake as a line (with $g = 1$ as the worst case).

The mean iris radius typical for the X-band RF structure installed at LCLS is $a = 4.7$ mm, the structure length is $L = 0.6$ m, the initial emittance is $\varepsilon_{N_0} = 0.6$ μm, the beta function in the structure is $\beta_0 = 11$ m, the fit parameter is $g \approx 2.5$, the electron energy is $E = 260$ MeV, the rms bunch length is $\sigma_z = 0.6$ mm, the bunch population is $N = 1.56 \times 10^9$, and the transverse misalignment is $x_0 = 0.17$ mm. From these numbers we use Eq. (91) to estimate an equivalent emittance growth of 6%, which is very close to the measured value of 7% shown in Fig. 16, and also shows the quadratic scaling with x_0. It is worth noting that the equivalent emittance growth scales with the 8^{th} power of the iris radius, a.

3.13 Transverse RF Deflector

Transverse RF deflectors can be used to separate electron bunches and distribute them to various destinations, such as applied at Jefferson Lab [23] and envisioned in the NGLS design [24]. Each bunch may be kicked left or right using one of the two RF crest phases (+90 or −90 deg), and the zero-crossing phase can also be used as a third direction (undeflected). However, in order not to significantly tilt the electron bunch from head to tail at the zero crossing-phase, the RF wavelength must be very long with respect to the bunch length. It is therefore useful to express the equivalent emittance growth for a bunch at the zero-crossing phase of an RF deflector in order to choose the upper limit of the RF frequency.

The kick angle of an electron at longitudinal position, z, along the bunch, from an RF deflector at a zero-crossing phase, but with a peak voltage, V_0, and wavelength, λ_{RF}, is given by $\Delta x' = \frac{eV_0}{E} \sin(2\pi z/\lambda_{RF})$, which for a bunch length much shorter than the reduced

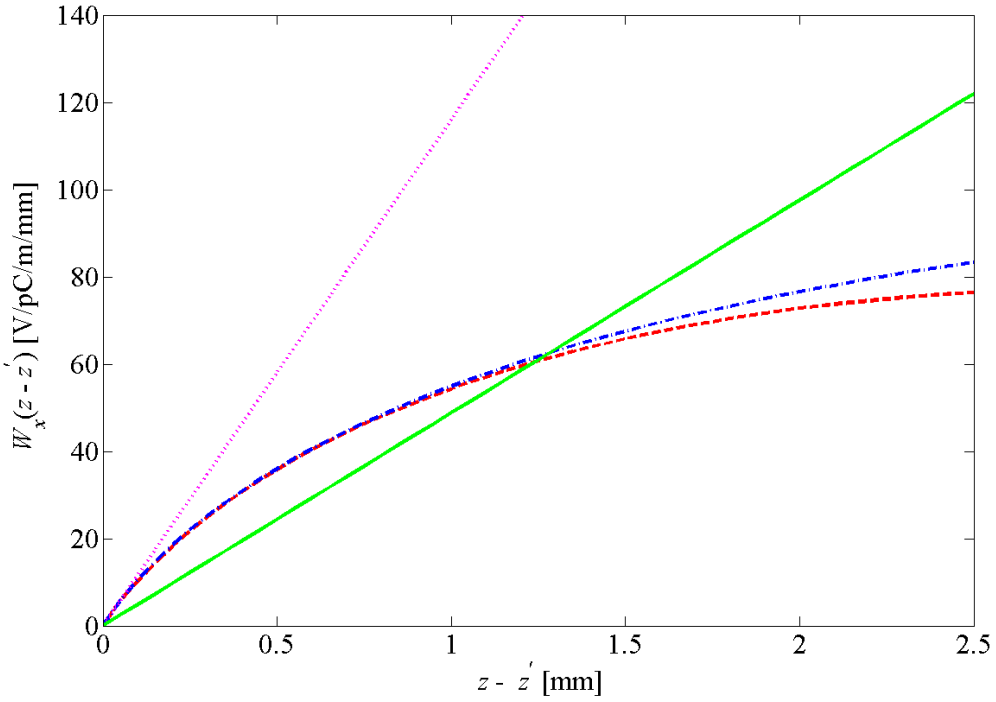

Figure 15: Point-charge dipole wake function for x-band RF structure with iris, $a \approx 4.7$ mm, and wake constant $s_1 \approx 0.4$ mm. The dashed red curve is a numerical calculation (most accurate here) while the dash-dot blue curve is Eq. (88), which approximates this wake over a 2.5-mm range (enough for our 0.6-mm rms bunch length). The solid green line is our linear approximation ($g = 2.5$), and the dotted magenta line is the slope evaluated at $z - z' = 0$ (by setting $g = 1$ in Eq. (89)). The wake is shown in volts per pC of bunch charge, per meter of structure length, and per millimeter of transverse offset.

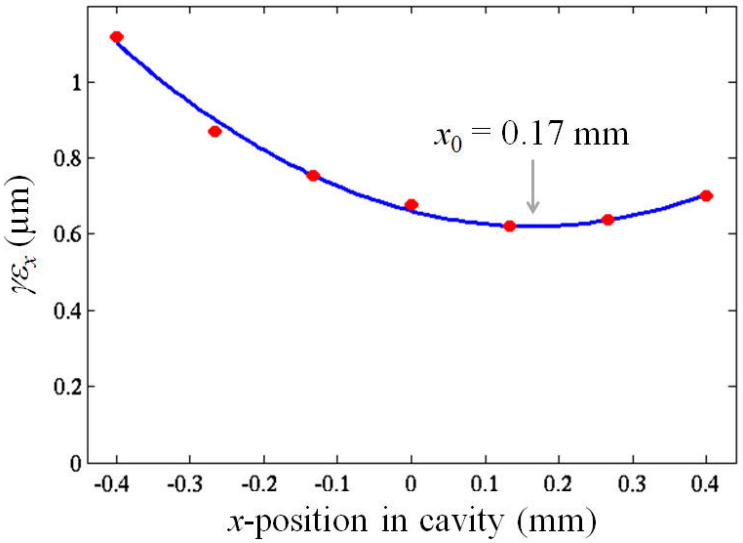

Figure 16: Measured normalized emittance after a 60-cm long X-band RF accelerating section at 260 MeV as the horizontal beam position, x, in the cavity is varied. The emittance is minimized at $x_0 = 0.17$ mm with a 7% increase at $x_0 = 0$.

RF wavelength ($\sigma_z \ll \frac{\lambda_{RF}}{2\pi}$) becomes $\Delta x' \approx 2\pi \frac{eV_0}{E} z/\lambda_{RF}$. Using Eq. (28) to calculate the equivalent emittance growth due to the RF deflector gives

$$\frac{\Delta\bar{\varepsilon}}{\varepsilon_0} \approx 2\pi^2 \frac{\beta_0}{\varepsilon_0} \frac{e^2 V_0^2}{E^2} \frac{\sigma_z^2}{\lambda_{RF}^2}. \tag{92}$$

As an example we take the NGLS beam spreader system which is based on transverse RF deflectors at 325 MHz ($\lambda_{RF} = 0.92$ m), with $V_0 = 3$ MV, $E = 2.4$ GeV, $\beta_0 = 15$ m, $\gamma\varepsilon_0 = 0.6$ μm, and $\sigma_z = 50$ μm. The equivalent emittance growth is 1%, which suggests choosing an RF frequency no higher than this 325-MHz level.

3.14 Tilted RF Accelerating Cavity

RF cavities are used to accelerate the electron beam to high energy, allowing efficient, short-wavelength FEL operation. A transversely misaligned cavity (or rigid group of cavities) can introduce a transverse wakefield, as discussed above. In addition, a tilted cavity (with pitch or yaw angle error) which is not operating at its crest phase, can kick the electron bunch differentially from head to tail, introducing a transversely tilted bunch (as an RF deflector) and therefore generates a projected emittance growth. It is therefore useful to estimate the equivalent emittance growth induced by a tilted RF accelerating cavity.

The kick angle of an electron at longitudinal position, z, along the bunch, from an RF accelerator with energy gain, eV_0, and wavelength, λ_{RF}, is given by $x' = \frac{eV_0}{E}\cos(2\pi z/\lambda_{RF} + \phi)\sin\theta$, where θ is the tilt-angle error of the cavity (a 'pitch' error in the vertical or 'yaw' error in the horizontal), and ϕ is the RF phase (with crest at $\phi = 0$). Note that we take the case where the energy gain over the RF cavity is small compared to the electron energy (with

E taken as the average energy over the cavity). For a small tilt error ($|\theta| \ll 1$), and an rms bunch length much shorter than the reduced RF wavelength ($\sigma_z \ll \frac{\lambda_{RF}}{2\pi}$), the kick becomes $x' \approx \frac{eV_0}{E}\theta(\cos\phi - 2\pi\frac{z}{\lambda_{RF}}\sin\phi)$. Here we are only interested in the differential kick across the bunch length (the z-dependent kick) so we ignore the first term as a static kick, easily removed by adjusting steering coils, and write the differential kick as $\Delta x' \approx 2\pi\frac{eV_0}{E}\theta\frac{z}{\lambda_{RF}}\sin\phi$, ignoring the sign. Again using Eq. (28) to calculate the equivalent emittance growth due to the tilted RF cavity gives

$$\frac{\Delta\bar{\varepsilon}}{\varepsilon_0} \approx 2\pi^2\frac{\beta_0}{\varepsilon_0}\frac{e^2V_0^2}{E^2}\frac{\sigma_z^2}{\lambda_{RF}^2}\theta^2\sin^2\phi, \tag{93}$$

which shows that the emittance growth is minimized with a short bunch, σ_z, a high energy, E, or an RF phase at crest, $\phi = 0$ (in this linear approximation). Note that we have ignored wakefields of the tilted cavity (addressed earlier) and assumed no significant cavity focusing.

As an example we take one 8-cavity, 1.3-GHz cryomodule at NGLS ($\lambda_{RF} = 0.23$ m), operating at an RF phase (ϕ) which is 25-deg off crest, with an 8-cavity total energy gain of $eV_0 = 120$ MeV, a mean beam energy of $E = 0.7$ GeV, $\beta_0 = 50$ m, $\gamma\varepsilon_0 = 0.6$ μm, and $\sigma_z = 400$ μm (before final compression). The equivalent emittance growth for a 0.5-mrad tilted cryomodule is 1%.

4 Example Tolerance Estimates

The following section applies a few of these emittance dilution formulas in order to estimate single component tolerances over the entire LCLS accelerator, including quadrupole magnet alignment, quadrupole and sextupole field component errors in dipole magnets, and roll angle tolerances of quadrupole magnets, etc. These tolerances are estimated based on a 2% emittance increase for each component, and using the 1-nC (2006) LCLS accelerator configuration (whereas the bunch charge is typically 150-250 pC since 2009, which further loosens these tolerances). Figures 17 and 18 show the optics functions along the accelerator, while Figures 19 through 21 show single component tolerances on a log scale for various errors as described in the captions.

5 Tabular Summary of Emittance Growth Formulas

The following table (2), for convenience, lists all of the emittance results derived above. Only the emittance growth in the dispersive-plane (horizontal) is shown here. When the error affects both planes (*e.g.*, a rolled quadrupole magnet) a second reference (to the other transverse plane) is included in the Eq. numbers at right.

6 Summary

Various transverse emittance dilution mechanisms are evaluated here with the 'equivalent' emittance definition introduced in order to simplify the formulation and include the induced

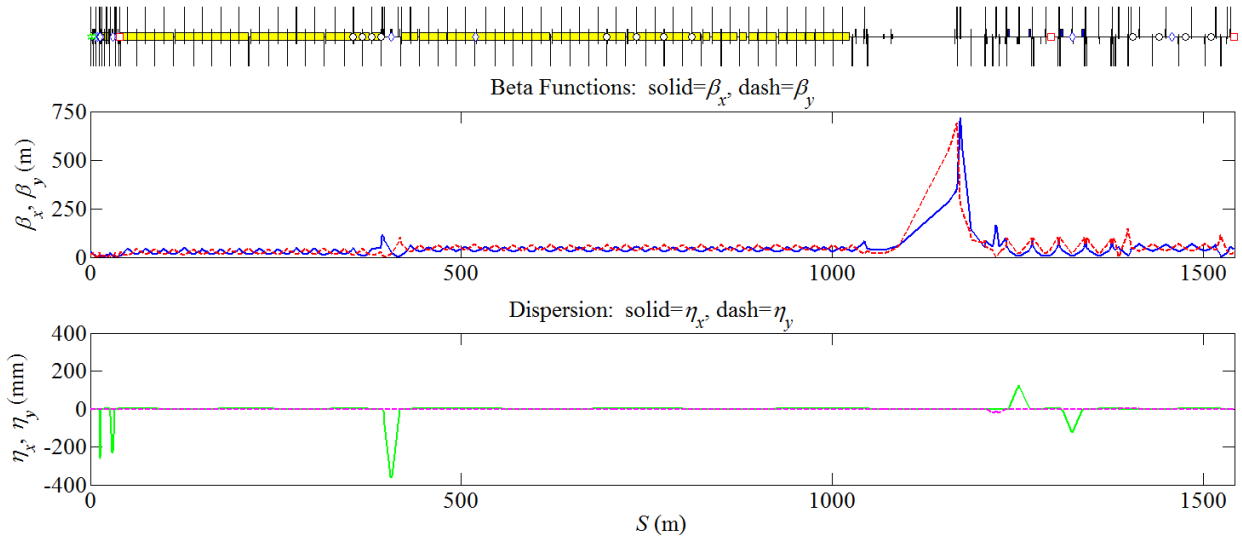

Figure 17: Beta functions (top) and dispersion (bottom) over the LCLS, up to the start of the undulator at 13.6 GeV. The horizontal beta function (top) is in solid-blue, while the vertical beta (top) is in dashed-red. Similarly the horizontal dispersion (bottom) is in solid-green, while the vertical dispersion (bottom) is in dashed-magenta.

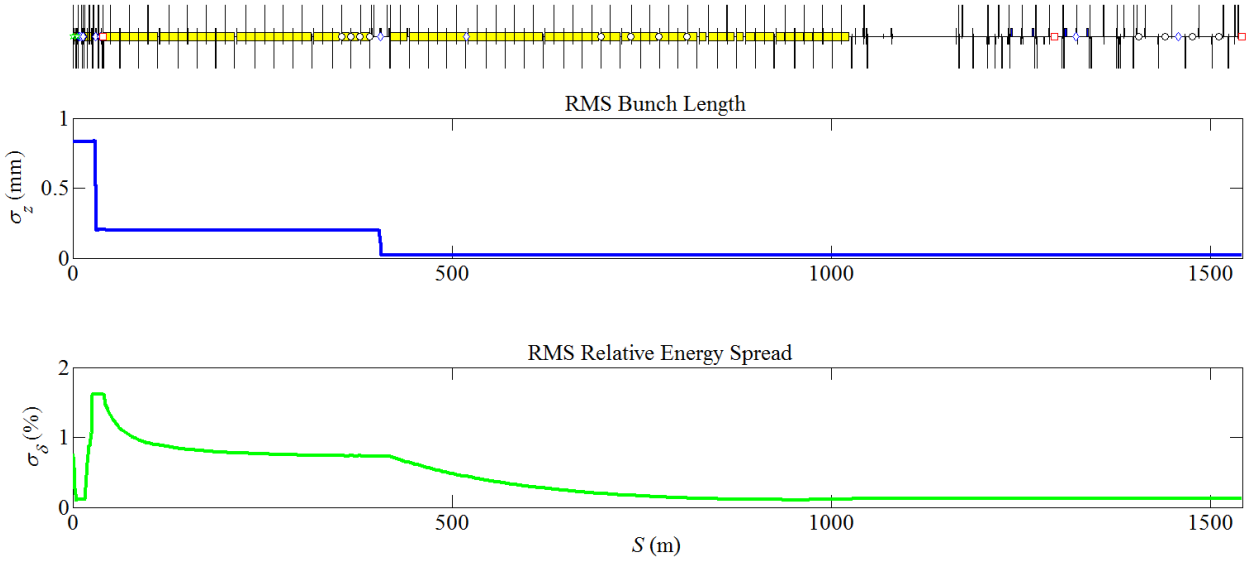

Figure 18: RMS bunch length (top) and rms relative energy spread (bottom) over the LCLS, up to the start of the undulator. The final rms relative energy spread is dominated by beam tails here. The core rms value is actually 0.01%. The final rms bunch length is 25 μm.

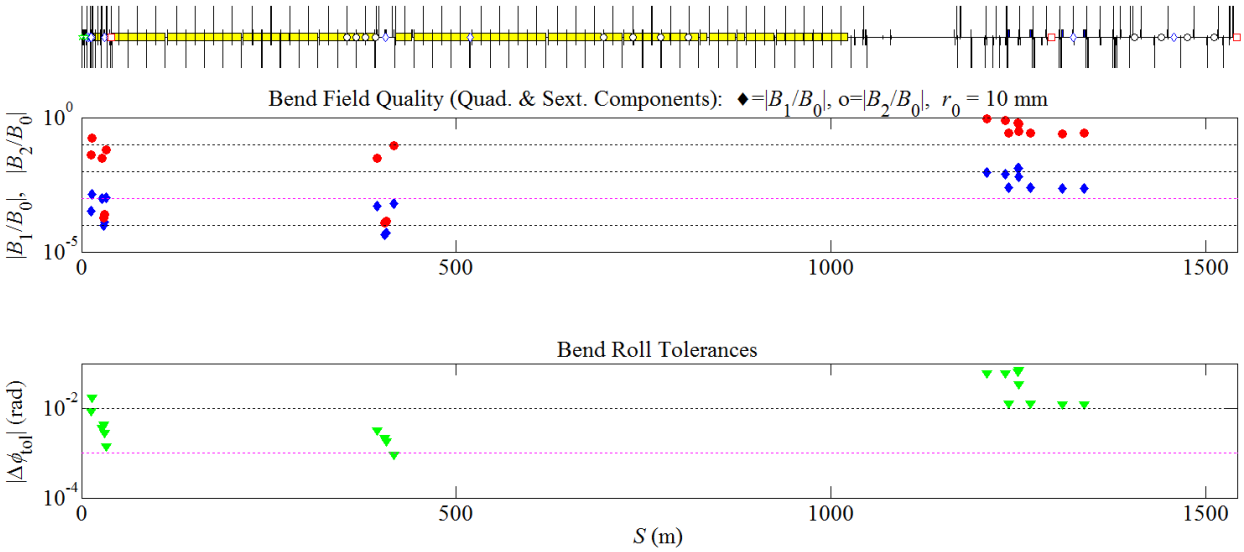

Figure 19: Quadrupole and sextupole field component tolerances for all dipole magnets (top) and dipole magnet roll angle tolerances (bottom) over the LCLS, up to the start of the undulator. Blue diamonds (top) are quadrupole field component tolerances, $|B_1/B_0|$, while red circles (top) are sextupole field component tolerances, $|B_2/B_0|$, for each dipole magnet and evaluated at a reference radius of $r_0 = 10$ mm. The tightest tolerances are the center BC2 dipoles with a gradient tolerance of $|B_1/B_0| < 5 \times 10^{-5}$ at a radius of $r_0 = 10$ mm.

matching error. Reasonably simple formulas are provided which relate accelerator component errors to beam brightness degradation, and can be used in tolerance estimations and for machine design considerations. These formulas are only approximate in most cases, but reflect the parameter scaling and allow quick estimates for single component errors. More detailed studies of multiple errors over a large machine are better suited to particle tracking in computer codes, some of which are used here for comparison and to validate these approximate formulas.

7 Acknowledgments

We especially thank Janos Hajdu for encouraging this work, along with Karl Bane, Michael Borland, Max Cornacchia, Dave Dowell, John Galayda, Zhirong Huang, Torsten Limberg, Thomas Lohse, Gennady Stupakov, Nick Walker, Frank Zimmermann, Max Zolotorev, and many others. Much of the work described here on transverse emittance preservation has greatly benefitted from long discussions with Bill Spence who was at SLAC during SLC operations in the 1990's. His ideas and mathematical methods were an inspiration and a solid platform from which to start this work.

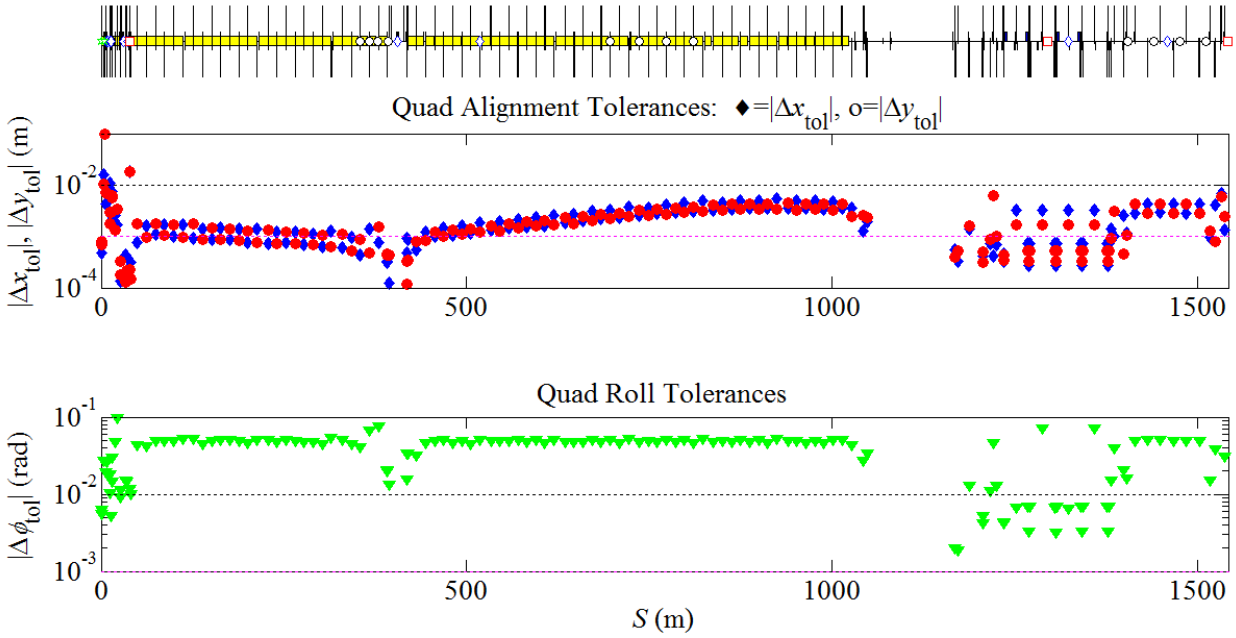

Figure 20: Transverse alignment tolerances (top) and roll angle tolerances (bottom) for all quadrupole magnets along the LCLS, up to the start of the undulator. Blue diamonds (top) are horizontal alignment tolerances, $|\Delta x_{tol}|$, while red circles (top) are vertical alignment tolerances, $|\Delta y_{tol}|$. The tightest alignment tolerances are two quadrupole magnets near the BC2 chicane, at $s \approx 400$ m, with alignment requirements at the 150 μm level, while the quadrupole magnet roll angle tolerances do not drop below 2 mrad.

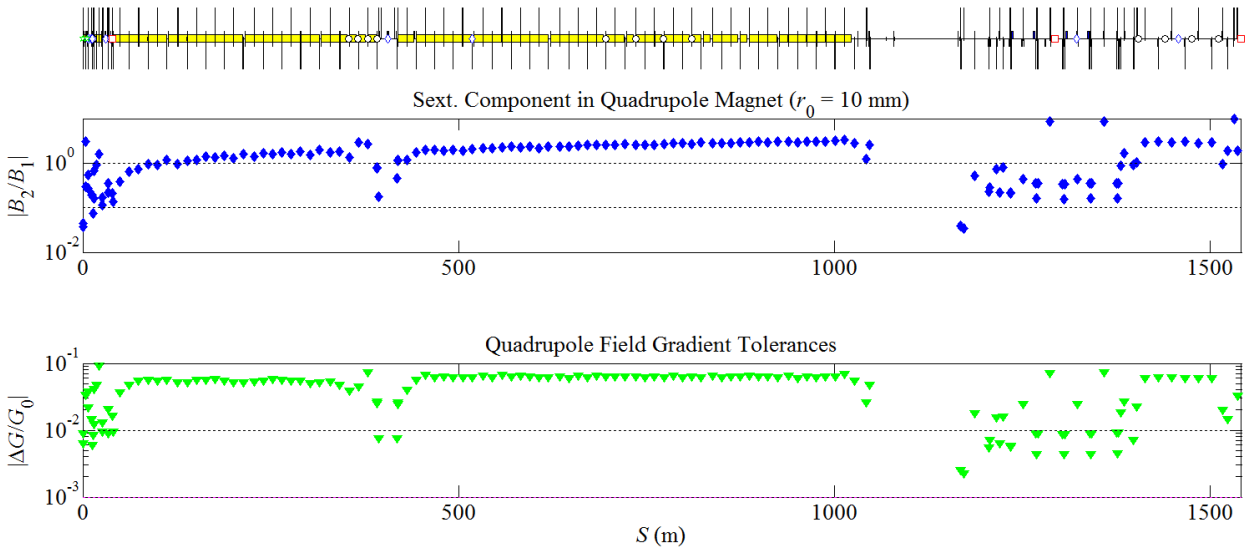

Figure 21: Sextupole field component tolerances in the quadrupole magnets (top) and relative field gradient tolerances for all quadrupole magnets (bottom) along the LCLS, up to the start of the undulator. Sextupole component tolerances are quite loose with $|B_2/B_1| > 4\%$ at $r_0 = 10$ mm, and quadrupole field gradient tolerances are typically above 1%, and do not drop below about 0.2%.

References

[1] P. Emma *et al.*, Nature Photonics, **4**, 641 (2010).

[2] J. Andruszkow *et al.*, Phys. Rev. Lett. **85**, 3825–3829 (2000).

[3] D. Pile, Nature Photonics, **5**, 456-457 (2011).

[4] Linac Coherent Light Source Conceptual Design Report, SLAC-R-593, 2002.

[5] K. L. Brown, "TRANSPORT: A Computer Program for Designing Charged Particle Beam Transport Systems", SLAC-91, May 1977.

[6] N. Merminga, P. L. Morton, J. T. Seeman, W. L. Spence, "Transverse Phase Space in the Presence of Dispersion", Proc. of the 1991 Part. Acc. Conf., p. 461, Washington, D.C., USA (1991).

[7] M. Sands, "A Beta Mismatch Parameter", SLAC-AP-85, April 1991.

[8] M.J. Syphers, T. Shen, D.A. Edwards, "Amplitude Function Mismatch", Proc. of the 1993 Part. Acc. Conf., p. 134, San Francisco, D.C., USA (1993).

[9] C. E. Adolphsen, P. J. Emma, T. H. Fieguth, W. L. Spence, "Chromatic Correction in the SLC Bunch Length Compressors", Proc. of the 1991 Part. Acc. Conf., p. 503, Washington, D.C., USA (1991).

[10] M. G. Minty and F. Zimmermann, *Measurement and Control of Charged Particle Beams*, Springer, Aug 5, 2003, Science, page 157.

[11] T. O. Raubenheimer, F.-J. Decker, J. T. Seeman,"Beam Distribution Function after Filamentation", Proc. of the 1995 Part. Acc. Conf., p. 3291, Dallas, Texas, USA (1995).

[12] CERN Accelerator School, Aarhus, Denmark, 15-26 Sep., 1986.

[13] Animesh K. Jain, Proc. CERN Accelerator School on Measurement and Alignment of Accelerator and Detector Magnets, April 11-17, 1997, Anacapri, Italy, CERN-98-05, pp. 1-26.

[14] K. L. Brown, "A Second-Order Magnetic Optical Achromat", SLAC-PUB-2257, Feb. 1979.

[15] P. Emma, K. Bane, M. Cornacchia, Z. Huang, H. Schlarb, G. Stupakov, D. Walz, Phys. Rev. Lett., **92**, 074801 (2004).

[16] Matthew Sands, SLAC-121, Nov. 1970.

[17] P. Emma and R. Brinkmann, Proc. of the 1997 Part. Acc. Conf., p. 1679, Vancouver, BC, Canada (1997).

[18] Y. S. Derbenev, J. Rossbach, E. L. Saldin, V. D. Shiltsev, "Microbunch Radiative Tail-head Interaction", TESLA-FEL 95-05.

[19] M. Borland, "Elegant: A Flexible SDDS-Compliant Code for Accelerator Simulation," Advanced Photon Source LS-287, Sep. 2000.

[20] Z. Huang *et al.*, Phys. Rev. Spec. Topics - Acc. and Beams **13**, 020703 (2010).

[21] K. L. F. Bane *et al.*, Phys. Rev. Spec. Topics - Accel. and Beams **12**, 030704 (2009).

[22] K. Bane, SLAC-PUB-9663 (2003).

[23] C. Hovater *et al.*, The CEBAF RF Separator System, LINAC-96, Geneva (CH), Aug. 26-30, 1996; JLAB-ACC-96-18.

[24] M. Placidi *et al.*, Proc. of the 2013 FEL Conf., New York, NY (2013).

Table 1: Most of the symbol definitions used throughout this note.

Parameter	**symbol**	**unit**
Initial rms emittance (hor. or ver.)	ε_0	m
Normalized rms emittance (hor. or ver.)	ε_{N_0}	m
Final rms emittance (hor. or ver.)	ε	m
Final rms equivalent emittance (hor. or ver.)	$\bar{\varepsilon}$	m
Electron energy	E	eV
Electron momentum	p	eV/c
Bunch population	N	
Electron's initial horizontal position	x	m
Electron's initial horizontal angle	x'	rad
Electron's initial vertical position	y	m
Electron's initial vertical angle	y'	rad
Electron's longitudinal position	z	m
Electron's relative energy deviation	δ	
Twiss beta function (hor. or ver.)	β	m
Twiss alpha function (hor. or ver.)	α	
Twiss gamma func. or Lorentz factor	γ	1 or 1/m
Hor. dispersion function (no ver.)	η	m
RMS bunch length	σ_z	m
RMS relative energy spread	σ_δ	
Amplitude of beta-mismatch (≥ 1)	ζ	see Eq. (9)
Dispersion to hor. beam size ratio	ξ	see Eq. (37)
Ver. to hor. beam size ratio	χ	see Eq. (47)
Dipole magnet bend angle or cavity tilt	θ	rad
Magnet or RF structure length	L	m
Bend radius of dipole magnet	ρ	m
Magnet roll angle error or RF phase	ϕ	rad
Quadrupole magnet focal length	f_0	m
Quadrupole magnet field gradient	G	T/m
Sextupole magnet strength	K_2	m^{-3}
Reference radius (field probe radius)	r_0	m
Radiation length of a foil	L_0	m
Iris radius of RF accelerating structure	a	m
Peak RF voltage	V_0	V
Wavelength of RF voltage	λ_{RF}	m
Speed of light	c	m/s
Free-space impedance	Z_0	Ohms
Classical electron radius	r_e	m
Planck's constant divided by 2π	$\hbar$	eV-s
Electron charge	e	C
Electron rest mass	mc^2	eV

Table 2: Summary list of emittance growth mechanisms, formulas, and Eq. numbers in the text. Only the emittance growth in the dispersive-plane (horizontal) is shown here. When the error affects both planes (*e.g.*, a rolled quadrupole magnet) a second reference (to the other transverse plane) is included in the Eq. numbers at right.

Mechanism	$\Delta\bar{\varepsilon}/\varepsilon_0 \approx$	**Eq.**
Angular Dispersion, θ_0	$\frac{1}{2}\frac{\beta_0}{\varepsilon_0}\theta_0^2\sigma_\delta^2$	29
Dipole Roll Error, ϕ	$\frac{1}{2}\frac{\beta_0}{\varepsilon_0}\phi^2\theta_0^2\sigma_\delta^2$	see 29
Spatial and Ang. Dispersion	$\frac{1}{2\beta_0\varepsilon_0}[\Delta\eta^2 + (\alpha_0\Delta\eta + \beta_0\Delta\eta')^2]\sigma_\delta^2$	31
Second-Order Dispersion	$\frac{2}{5}\frac{1}{\beta_0\varepsilon_0}[\Delta\eta_2^2 + (\alpha_0\Delta\eta_2 + \beta_0\Delta\eta_2')^2]\sigma_\delta^4$	33
Third-Order Dispersion	$\frac{27}{14}\frac{1}{\beta_0\varepsilon_0}[\Delta\eta_3^2 + (\alpha_0\Delta\eta_3 + \beta_0\Delta\eta_3')^2]\sigma_\delta^6$	34
Quadrupole Gradient Error	$\frac{1}{2}\left(\frac{\Delta G}{G_0}\right)^2\frac{\beta_{x0}^2}{f_0^2}(1+\xi^2)$	35,36,37
Quad. Transverse Offset, x_0	$\frac{1}{2}\frac{\beta_{x0}}{\varepsilon_{x0}}\left(\frac{x_0}{f_0}\right)^2\sigma_\delta^2$	38
Quad. Roll Angle, ϕ	$\frac{1}{2}\sin^2(2\phi)\frac{\beta_{x0}\beta_{y0}}{f_0^2}\left(\frac{\varepsilon_{y0}}{\varepsilon_{x0}}\right)$	39,40
Sextupole Trans. Offsets, x_0, y_0	$\frac{1}{2}K_2^2L^2\beta_{x0}^2\left[x_0^2(1+\xi^2) + y_0^2\chi^2\right]$	45,46,37,47
Skew Quadrupole Coupling	$\frac{1}{2}\left(\frac{\varepsilon_{y0}}{\varepsilon_{x0}}\right)\frac{\beta_{x0}\beta_{y0}}{f_0^2}$	48,49
Quad. Field Error in Dipole	$\frac{1}{2}\theta_0^2\left(\frac{B_1}{B_0}\right)^2\frac{\beta_{x0}^2}{r_0^2}(1+\xi^2)$	51,52,37
Sext. Field Error in Dipole	$\theta_0^2\left(\frac{B_2}{B_0}\right)^2\frac{\beta_{x0}^3\varepsilon_{x0}}{r_0^4}\left[(1+\xi^2)^2+\chi^4\right]$	57,58,37,47
Chromaticity of Quad.	$\frac{1}{2}\frac{\beta_{x0}^2}{f_0^2}\left(1+2\xi^2\right)\sigma_\delta^2$	60,61,37
Sextupole Aberration	$\frac{1}{4}K_2^2L^2\beta_{x0}^3\varepsilon_{x0}\left[(1+\xi^2)^2+\chi^4\right]$	62,63,37
Coulomb Scattering	$\frac{1}{2}\frac{\beta_0}{\varepsilon_0}\frac{E_0^2}{E^2}\frac{L}{L_0}\left(1+\frac{1}{9}\log_{10}\left(\frac{L}{L_0}\right)\right)^2$	65
ISR in 4-Dipole Chicane	$\frac{55}{144\sqrt{3}}\frac{r_e\hbar c}{(mc^2)^7}\frac{E^6\lvert\theta_0^5\rvert}{\varepsilon_{N_0}L^2}\left(4\beta_0 + 4\alpha_0L_T + \gamma_0\frac{\Lambda^2}{10}\right)$	78,77
CSR in Last Chicane Dipole	$0.024\frac{r_e^2N^2}{\varepsilon_{N_0}}\frac{mc^2}{E}\left(\frac{L\lvert\theta_0^5\rvert}{\sigma_z^4}\right)^{2/3}\left(\frac{\beta_0}{4}+\frac{\alpha_0L}{6}+\frac{\gamma_0L^2}{36}\right)$	84
Energy Modulation in Chicane	$\frac{1}{2}\left(1+\alpha_0^2\right)\frac{\eta^2}{\varepsilon_0\beta_0}\sigma_\delta^2$	86
Transverse RF Wakefields	$\frac{2\beta_0}{\varepsilon_0}\left(\frac{Z_0cNe^2Lx_0}{\pi gEa^4}\right)^2\sigma_z^2$	91
Transverse RF Deflector	$2\pi^2\frac{\beta_0}{\varepsilon_0}\frac{e^2V_0^2}{E^2}\frac{\sigma_z^2}{\lambda_{RF}^2}$	92
Tilted RF Acc. Cavity	$2\pi^2\frac{\beta_0}{\varepsilon_0}\frac{e^2V_0^2}{E^2}\frac{\sigma_z^2}{\lambda_{RF}^2}\theta^2\sin^2\phi$	93